



eBook

Signal Integrity Tips and VNA Measurements

December 2019

SPONSORED BY



3

Introduction

Pat Hindle
Microwave Journal, Editor

4

Signal Integrity Tips and Techniques Using TDR, VNA and Modeling

Heidi Barnes, Jeff Most, and Mike Resso

10

Time Domain Analysis with Copper Mountain Technologies Vector Network Analyzers (VNA)

Copper Mountain Technologies

29

Characterizing Uncertainty in S-Parameter Measurements

Tekamul Buber, Pragti Narang, Giampiero Esposito and Sathya Padmanabhan
Maury Microwave, Ontario, Calif.

Markus Zeier
Federal Institute of Metrology (METAS), Berne-Wabern, Switzerland

35

Using a VNA for Power Plane Impedance Analysis

Brian Walker
Copper Mountain Technologies

39

1.35 mm Precision Coaxial Connector Enables High Performance E-Band Cable Assemblies

Daniel Barnett
Teledyne Storm Microwave, Woodridge, Ill.

Hans-Ulrich Nickel
SPINNER GmbH, Munich, Germany

Signal Integrity Tips and VNA Measurements

Signal integrity addresses the losses and types of signal degradation that can happen along the signal path (channel) between a transmitter and a receiver. Signal integrity is becoming more and more important as digital signal speeds and analog frequencies are rapidly increasing making circuits much more sensitive to any losses or variations in the path. This eBook provides information and instruction on making accurate signal integrity measurements with emphasis on the VNA as a tool.

The first article is about Signal Integrity tips and techniques using TDR, VNA and modeling to understand the channel design. The next article covers time domain analysis using Copper Mountain VNAs. It provides a nice review of the theory and methods of measurements in detail.

Those articles are followed by one about characterizing uncertainty in S-Parameter measurements so you can see what parameters affect the accuracy of your measurements and how to improve them. Then we have an article about using a VNA for power plane impedance analysis as power supplies have become a critical component in the design of high frequency and high-speed circuits.

Finally, we end with an article about the design of 1.35 mm precision coaxial connector that enables high performance E-Band cable assemblies for accurate measurement of high frequency and high-speed signals showing the importance of the connection signal integrity.

We thank Copper Mountain for sponsoring this eBook so you can download and read it at no cost. Copper Mountain has a wide range of low cost, high performance VNAs and have been working with many companies in the industry to come up with total measurement solutions for measuring materials, antennas, devices and circuits.

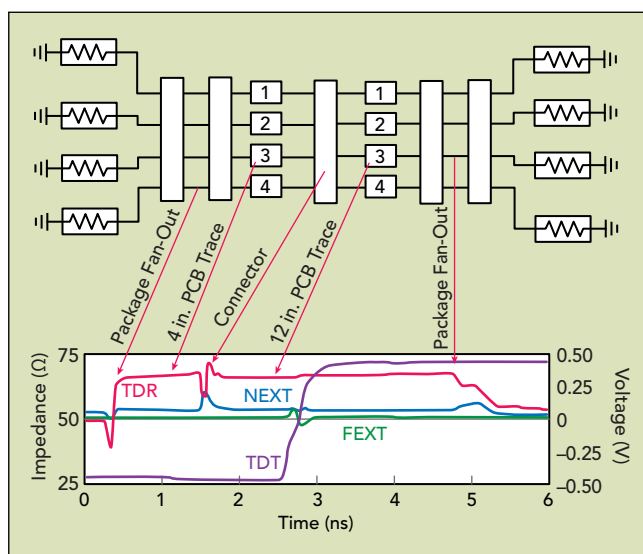
Pat Hindle, Microwave Journal Editor

Signal Integrity Tips and Techniques Using TDR, VNA and Modeling

Heidi Barnes, Jeff Most, and Mike Resso

Signal integrity (SI) is all about the losses and types of signal degradation that can happen along the path (channel) between a transmitter and a receiver. In a perfect world, transmitter communication would instantaneously be heard at the receiver and with no change in the signal. Equalization methods exist both in the transmitter and the receiver to help correct for channel losses, but they have their limitations,

and the channel must still have some minimal level of performance. SI engineers are faced with the challenge of how to characterize the signal losses that exist in the channel and identify the key elements that are controlling the performance. The use of time and frequency domain analyses for both simulation and measurements is a fast way of becoming an expert on a given channel design.



▲ Fig. 1 Distributed model of the physical channel and the resulting TDR and TDT.

SIMULATION MODELING

Starting with simulation, one can build a distributed model of the channel with measurements, EM simulations and/or algorithmic models that are cascaded together to predict channel performance. One can look at the output eye diagram to see the aggregate performance and do brute force simulations by varying hundreds of variables to find the best performance. The better option is to run quick time and frequency domain analyses to gain insight and reduce the design space that needs to be simulated. **Figure 1** shows how time domain reflectometry (TDR) and transmissivity (TDT) can be used to get spatial information on what is happening to the signal as it travels through the channel. The TDR shows where reflections are occurring, which reduces the amount of signal that reaches the transmitter. The TDT shows how the rise time is degraded by material losses in the channel. The near end cross talk (NEXT) on adjacent channels shows which component is the likely source of noise coupling, by being coincident in time with the component's TDR reflection.

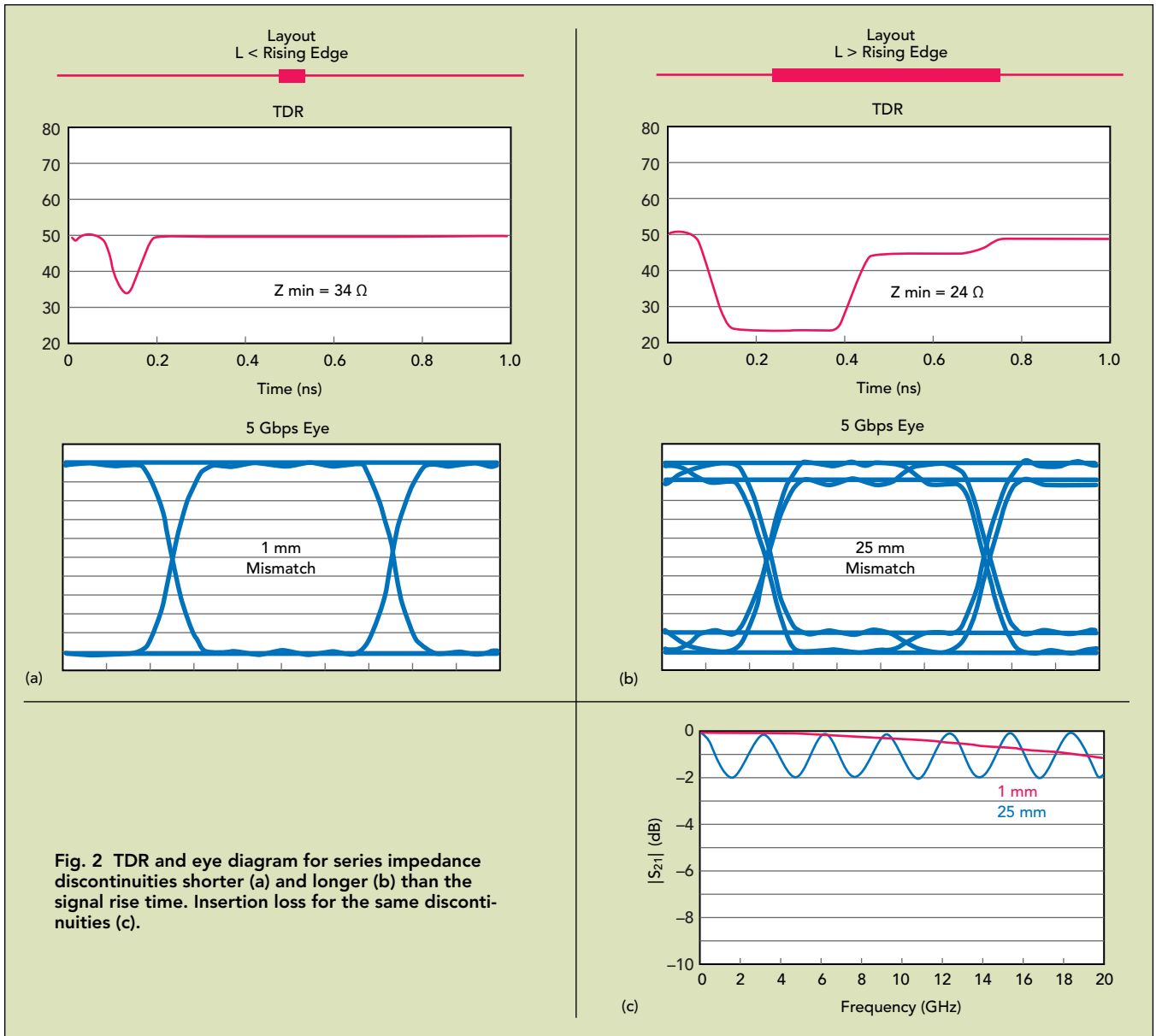


Fig. 2 TDR and eye diagram for series impedance discontinuities shorter (a) and longer (b) than the signal rise time. Insertion loss for the same discontinuities (c).

This is a very high level look at the power of time domain analysis. To become an expert at reading the TDR/TDT and frequency dependent losses, some very simple simulations can help. The two basic types of impedance discontinuities encountered in a channel are a series change in impedance and a stub that branches off the signal path. Simulating the series impedance discontinuity from a length that is shorter than the rise time of the signal to a length that is much longer shows two very different responses in the time and frequency domain. As the length of the discontinuity gets shorter than the rise time of the signal, the reflection gets smaller and more of the signal transmits through (see **Figure 2a**). At longer lengths, the double reflections off both ends of the series impedance discontinuity result in a forward traveling wave that is delayed in time and added back into the signal going to the receiver (see **Figure 2b**). This causes a rippling in the amplitude of the signal versus frequency. The ripple valleys are located at frequencies where the forward traveling waves

are 180 degrees out of phase and destructively add (see **Figure 2c**).

The stub resonator exhibits some of the same behavior. When the stub is much shorter than the rise time, the reflection is reduced, and more of the signal goes through to the receiver (see **Figure 3a**). A stub longer than the rise time (see **Figure 3b**) can lead to significant losses, where 100 percent reflection from the end of the stub destructively adds with the forward traveling wave (see **Figure 3c**).

Simulation makes it easy to create a stub and series impedance discontinuity with the same excess capacitance and delta impedance change, to see how these two types of structures compare in the time and frequency domain. It is not just the TDR peak height that matters, but also the subtle information from the double reflection occurring later in time. With these two simple simulations, an SI engineer can look at an eye diagram at the receiver, an S-parameter frequency response or a TDR/TDT time domain response and know whether the problem is a series or stub impedance discontinuity.

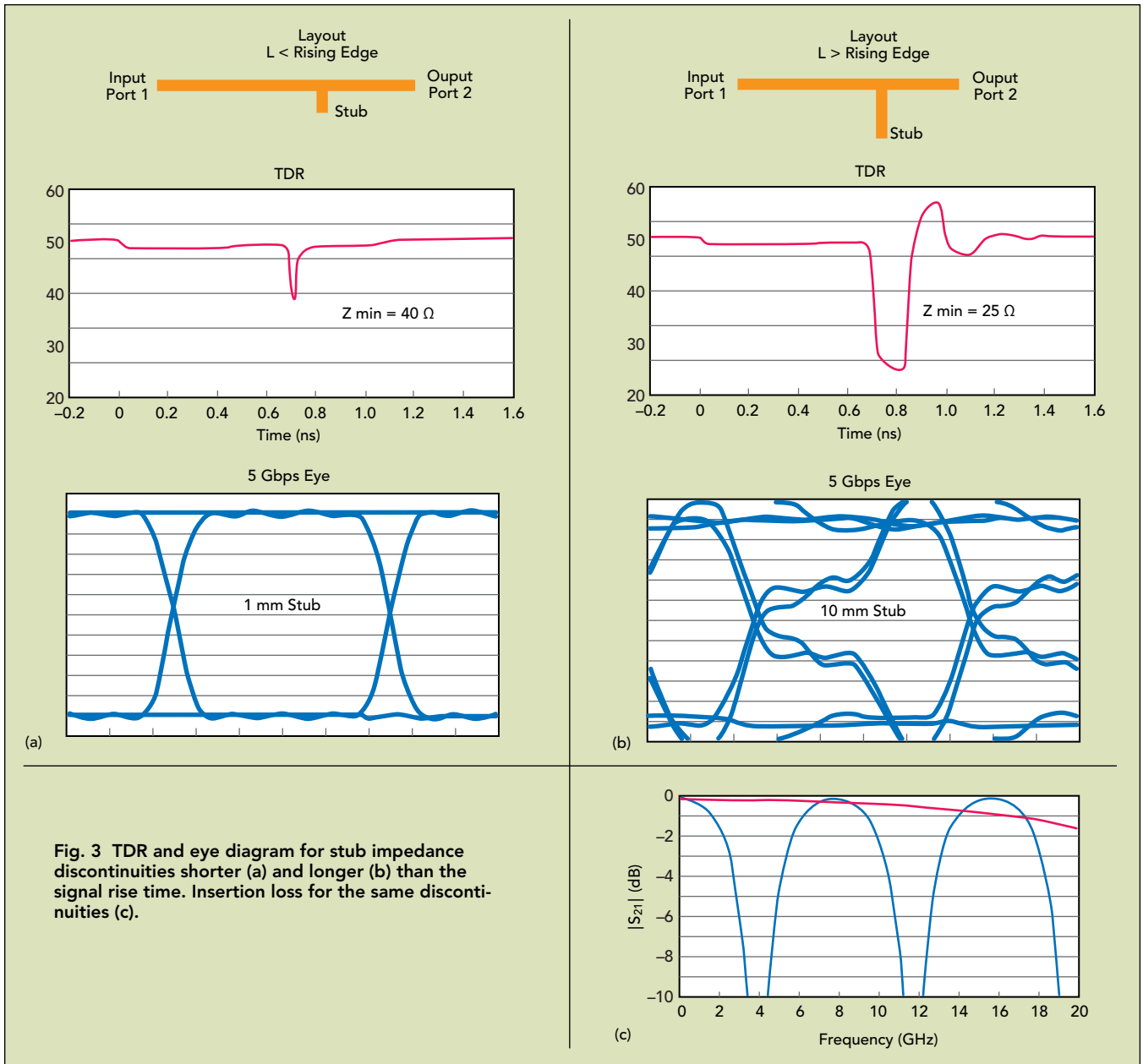
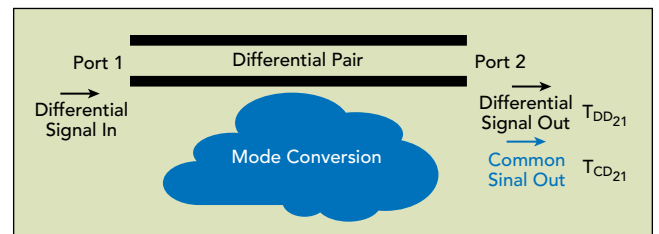


Fig. 3 TDR and eye diagram for stub impedance discontinuities shorter (a) and longer (b) than the signal rise time. Insertion loss for the same discontinuities (c).

FINDING CAUSES OF EMI

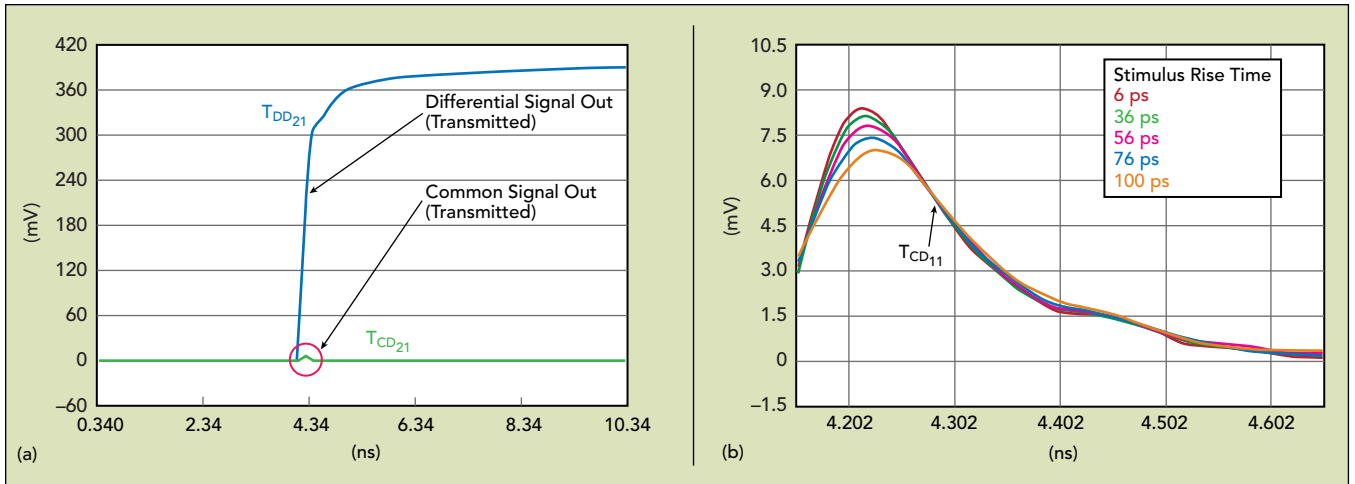
The spatial information that TDR/TDT provides can also be used for understanding and troubleshooting EMI problems coming from the physical channel. While there are many potential sources of EMI in high speed serial designs, the most typical is radiation caused by common currents generated by a differential channel. A common signal as small as 10 mV on an external twisted pair can cause an FCC certification test failure. In theory, if the drivers produce a perfect differential signal and the signal passes through a perfect differential channel, there will be no common signal generated. Unfortunately, in practice that is seldom the case.

Assuming the driver is perfect and considering just the channel, any asymmetry in a coupled differential channel will convert some of the differential signal into a common signal. This is known as "mode conversion" (see **Figure 4**). Mode conversion is typically caused by asymmetries in the coupled lines, such as non-equal

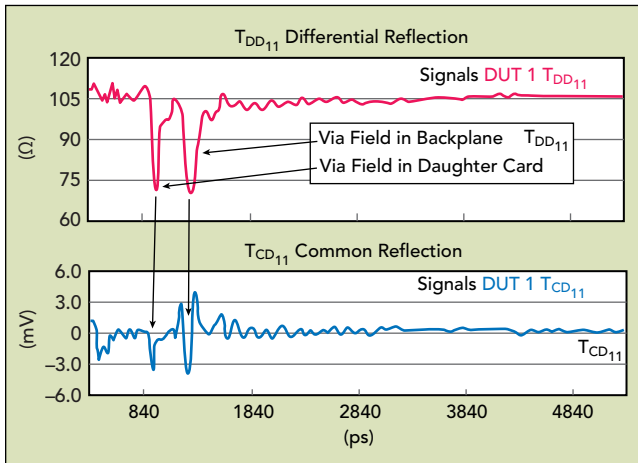


▲ Fig. 4 Asymmetry in a coupled differential transmission line will create a common signal at the output.

line widths and/or lengths, different "local" effective dielectric constants, or ground-plane discontinuities. TDR can help in two ways. The first is to determine if mode conversion exists. Using TDR, the channel at port 1 is stimulated with a differential signal and the common mode response at port 2 is measured. **Figure 5** shows the measured results from a typical backplane. Three conclusions can be drawn from these test results:



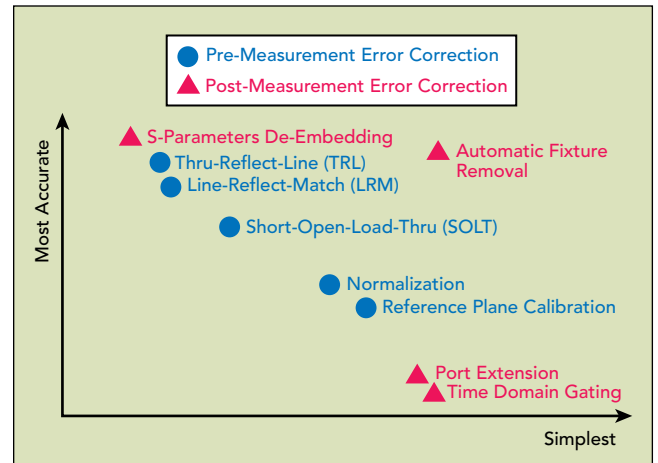
▲ Fig. 5 Measured TDT response of a backplane, showing the differential and common responses (a) and magnified view of the common responses vs. stimulus rise times (b).



▲ Fig. 6 Using TDR to find the cause of mode conversion.

- There is mode conversion in the channel
- The common signal and differential signal travel at similar, yet not exactly the same velocities
- The edge speed of the differential stimulus has a small impact on the mode conversion.

The second way TDR can help is to look at the reflected signal to determine what in the device under test (DUT) is causing mode conversion. **Figure 6** shows the measurement when stimulating the DUT with a differential signal at port 1 and measuring both the differential and common reflected signals at port 1. As the stimulus propagates through the channel, any asymmetry encountered will generate a common signal. Some of that common signal will propagate to port 2 and some will propagate to port 1, where it is measured as TCD11. Because the velocity of the common signal is similar to the velocity of the differential signal, features in the impedance profile coincident with the common signal can be used to determine the cause of the mode conversion. In this case, mode conversion is caused by the via fields in the daughter card and backplane.



▲ Fig. 7 Assessment of the numerous error correction techniques for removing fixture effects on the DUT measurement.

FIXTURE EFFECTS

Finally, key to the success of distributed channel simulation and measurement is the ability to measure just the DUT. At high frequencies this can be quite challenging, as the fixture starts to become a significant source of signal degradation, requiring advanced calibration techniques to remove the fixture from the measurement.

Many different approaches have been developed for removing the effects of the test fixture from the measurement; these fall into two categories: direct measurement (a pre-measurement process) and de-embedding (post-measurement processing). De-embedding uses a model of the test fixture and mathematically removes the fixture characteristics from the overall measurement. This fixture de-embedding procedure can produce very accurate results for the non-coaxial DUT without complex, non-coaxial calibration standards. Direct measurement techniques require specialized calibration standards that are inserted into the test fixture and measured. The accuracy of the device measurement relies on the quality of these physical standards (see **Figure 7**).

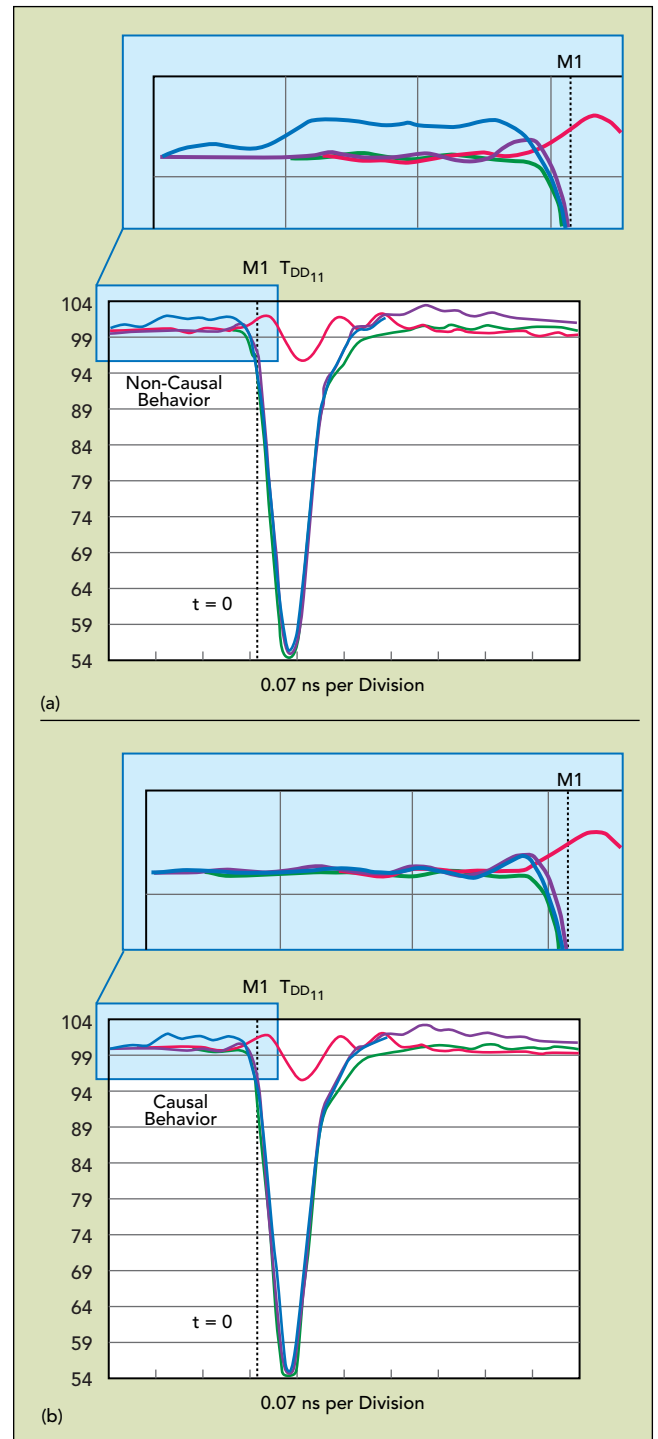
The most common calibration methodology is called TRL, for transmission (or thru), reflect and line. The constraints for the TRL standards are that the connectors and launches are all identical and all the transmission lines used for the thru and line standards have the same impedance, loss and propagation constant — only varying in length. The number of lines needed will depend on the frequency range covered by the calibration kit. The usable frequency range for each line is determined by comparing the phase of the line standard to the thru standard. Microwave test applications have used TRL calibration techniques for over 40 years with vector network analyzers (VNA). The TRL calibration technique relies only on the characteristic impedance of a short transmission line. From two sets of two-port measurements that differ by this short length of transmission line and two reflection measurements, the full 12-term error model can be determined. Due to the simplicity of the calibration standards, TRL can be applied in dispersive transmission media such as microstrip, stripline and waveguide. With precision coaxial transmission lines, TRL has provided the highest accuracy in coaxial measurements since 1975.

A recently developed calibration method called differential cross talk calibration (also referred to as differential TRL) is a differential version of the common, single-ended TRL, using differential instead of single-ended structures. Differential TRL is one of the few calibration algorithms, along with automatic fixture removal (AFR) that accounts for and removes coupling. The same constraints as the single-ended TRL described earlier apply to this differential method. Since these are differential standards, there are additional constraints: mode conversion, whether it be common to differential or differential to common, should be -30 dB or better. The skew between lines needs to be less than 10 degrees. As with single-ended TRL calibration kits, the fixture may be asymmetric (left and right half fixtures do not need to be the same length or impedance), but the fixtures need to be symmetric top to bottom (i.e., one leg to the other leg of the differential pair).

The latest generation AFR algorithms are often referred to as "one-port AFR." This reference to one-port can be either a single-ended port or differential port, but in either case there is no thru measurement required. This enables much simpler and straightforward error correction, because the user can simply use the open ended fixture as a reference standard, saving design time and fabrication costs. Similar to the single-ended AFR, there is a differential automatic fixture removal method. The difference in this method is that the thru is differential; therefore, any coupling that exists in the fixture is also removed in the process. Besides needing to be symmetric (right to left), like the single-ended AFR the thru must also be symmetric top to bottom. Like the single-ended version, this takes less to implement and build than the related multiple TRL structures.

A design case study was conducted to show an application where the $2\times$ thru fixture was manufactured with typical PCB manufacturing tolerances of ± 10 percent of the target impedance. This means the differential impedance of 100 V can be as high as 110 V or as low as

90 V, up to a 20 V spread in $2\times$ thru impedance and, more importantly, a significant difference between the fixture to be removed and the $2\times$ thru that is fabricated. Normally, one of the main assumptions in TRL and AFR is that the fixture and calibration $2\times$ thru standard have identical impedance. Another breakthrough in calibration algorithms now exists, where impedance differences between the fixture and the calibration $2\times$ thru standard can be tolerated. This provides new flexibility



▲ Fig. 8 Before (a) and after (b) TDR responses, showing the reduction in non-causal behavior using the enhanced AFR algorithm.

that improves accuracy and reduces implementation time by avoiding multiple board turns of the calibration 2× thru standard. This enhanced AFR algorithm will take the original measurement of fixture A + DUT + fixture B and compare it to the 2× thru. By specifying that the characterization fixture does not equal the DUT measurement fixture, AFR will use the actual fixture impedance and allow the proper impedance to complete the error correction methodology. The causality problem of having some erroneous response before time $t = 0$ is greatly reduced (see **Figure 8**). This novel feature offers another breakthrough for automatic fixture removal and S-parameter accuracy.

Signal integrity engineers have many tools available in the lab to make life easier.¹ Microwave transmission line knowledge, calibration and error correction techniques, and time domain intuition all play an important role in identifying and resolving the root cause of problems. Simulation plus measurement techniques can help provide insight into the success of high speed serial channels. ■

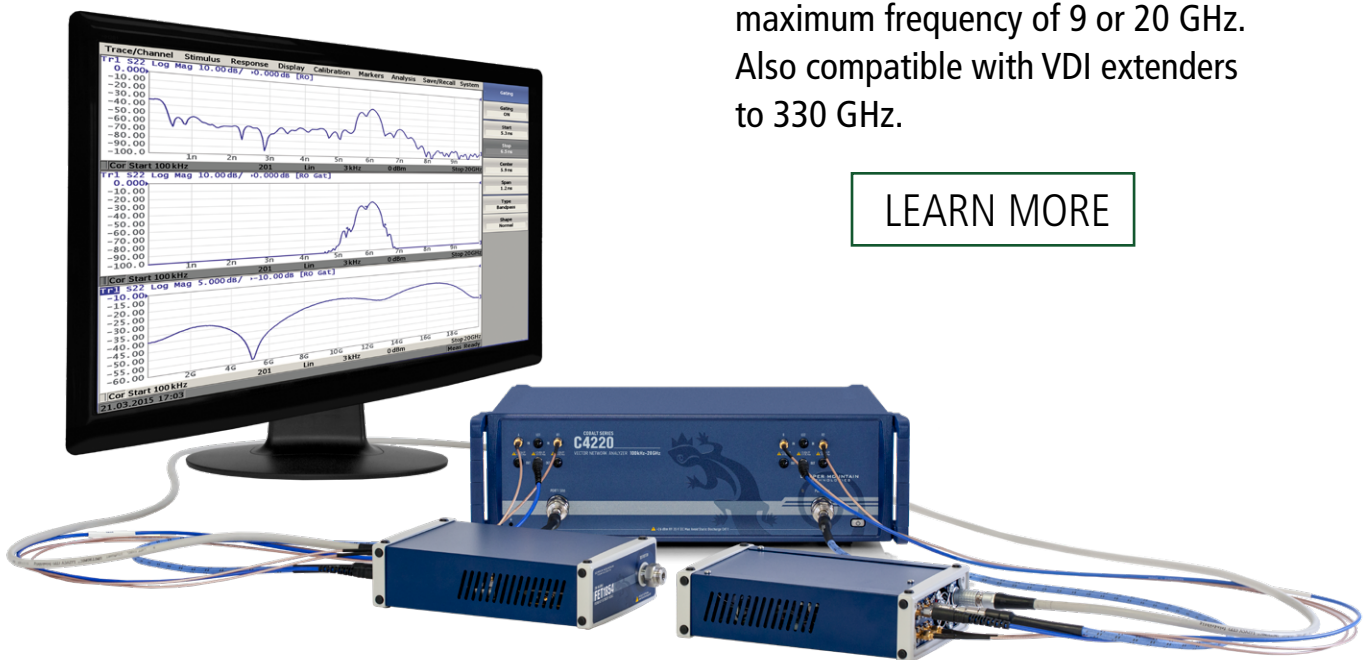
Reference

1. Mike Resso and Eric Bogatin, "Signal Integrity Characterization Techniques," 2nd edition, International Engineering Consortium.

CobaltFx mmWave Frequency Extension System

CobaltFx allows you to build a scalable and affordable 5G testing solution, offered with four extension frequency band options from 18-110 GHz. The system can be anchored by 2- or 4-port Cobalt VNAs with a maximum frequency of 9 or 20 GHz. Also compatible with VDI extenders to 330 GHz.

LEARN MORE



COPPER MOUNTAIN
TECHNOLOGIES

TIME DOMAIN ANALYSIS WITH COPPER MOUNTAIN TECHNOLOGIES VECTOR NETWORK ANALYZERS (VNA)

Contents

| | |
|--|-----------|
| INTRODUCTION | 11 |
| BRIEF THEORY | 11 |
| SETTINGS | 12 |
| Frequency Domain Settings | 12 |
| Frequency Span | 12 |
| Points | 13 |
| Time Domain Settings | 13 |
| Transformation Type:..... | 13 |
| Windowing | 15 |
| Velocity Factor | 18 |
| TIME DOMAIN GATING | 19 |
| ACCURACY CONSIDERATIONS | 21 |
| COMMON APPLICATIONS | 22 |
| A: Impedance on a PCB line | 22 |
| B: DTF on a long cable | 23 |
| C: High speed differential measurements | 25 |
| Conclusion | 28 |
| References | 28 |



COPPER MOUNTAIN
TECHNOLOGIES

www.coppermountaintech.com

INTRODUCTION

A Vector Network Analyzer (VNA) natively measures complex S-parameters of a device under test (DUT) in the frequency domain mode by sweeping across various frequency points. While there is an exhaustive list of measurements that can be accomplished in the standard frequency domain mode – using the advanced inverse Chirp z-transformation, the measurements can also be simultaneously analyzed in the time domain mode. This gives the added advantage where the two fundamental modes of analysis can be performed by one single instrument.

A VNA with its highly accurate vector error correction method can precisely locate the mismatches just like a traditional Time Domain Reflectometer (TDR) would. Although both instruments provide frequency and time domain using Fourier transform, they work differently in terms of the principle operation. Unlike a TDR where it sends a step or an impulse down the transmission line and compares the reflected signal with a wideband oscilloscope, a VNA uses narrowband tuned receivers to compare the swept frequency signal, thereby paving way to achieve better signal to noise ratio. Creating a higher dynamic range, which is useful for a lot of measurements, even in the time domain mode.

For an RF/Microwave engineer, time domain measurements are primarily useful in identifying a device's behavior at specific locations. And more recently, with the increasing necessity of high-speed applications, VNAs are also gaining popularity with digital engineers for signal integrity tests.

Note: All Copper Mountain Technologies' VNAs, except the compact M Series, come with time domain and gating as a standard feature in the VNA application software.

BRIEF THEORY

Fourier transform is a powerful tool which makes the frequency and time domain transformations possible. These transformations are performed by analyzing the impulse and step responses of a network. Various fast Fourier transform (FFT) algorithms are used in test and measurement instruments due to its superior computation times when compared to discrete Fourier transform (DFT). However, as the VNA measures discrete magnitude and phase of the DUT over a finite frequency range, there are some limitations on the transformations that can be applied. So, a proprietary chirp z algorithm is used. The advantage of using chirp z is that it offers greater flexibility in evaluating the z-transform along contours other than the unit circle, as the input and output samples do not have to be the same. This essentially allows the user to zoom into the desired area on the time domain axis.

From [1], for a given N -sample sequence, the chirp z-transform is defined as:

$$X(k) = \sum_{n=0}^{N-1} x[n] (A \cdot W^{-k})^{-n}$$

Where $X(k)$ is the transformed response for the given N -sample sequence $x[n]$ sampled in M points ($0 \leq k \leq M - 1$). Here A and W are arbitrary complex numbers defined as:

$$A = A_0 e^{i2\pi\theta_0}$$

$$W = W_0 e^{-j2\pi\varphi_0}$$

Where A_0 is the starting radius, θ_0 is the starting angle and φ_0 is the angular step size. The rate at which the contour spirals in or out from the circle of radius A_0 is set by the constant W_0 . The $A W^{-k}$ term configures the contour at which the z-transform is defined.

Besides this, there are additional functions to be considered prior to applying transformation such as: low pass (where the DC and negative frequencies are extrapolated to simulate TDR) & bandpass modes (for band limited DUTs) and windowing (to truncate the signal) to name a few. Users can adjust these settings to best suit their application. As the focus of this application note is not to delve into the underlying algorithm, the next section shows how these, and other settings affect the time domain transformations in a VNA.

SETTINGS

Time domain transformations are trace wise operations performed on an active trace when the sweep type is set to linear. To accomplish the desired time domain measurements for various applications, appropriate settings must be used.

Frequency Domain Settings

Frequency Span

Resolution in time domain is inversely proportional to the frequency span of the VNA setting. So, the wider the frequency, the better the resolution is. In addition to the frequency span settings, the window settings (discussed later) also determine the resolution in time domain mode:

$$\text{Resolution (in distance)} \approx \frac{V_p * C}{2 * (Fmax - Fmin)}$$

Where V_p is the velocity factor of the transmission line

C is the speed of light

$Fmax$ & $Fmin$ are the maximum and minimum frequency from the VNA

In general, to achieve higher resolution, the full range of the VNA must be utilized even if the frequencies are outside the DUT's working range. This is valid as long as the DUT is not band limiting such as filters or waveguides.

Points

Range in time domain, is directly proportional to the number of frequency points and inversely proportional to the frequency step size of the VNA setting. So, to measure longer distances, it is necessary to set many frequency points. Here is the equation to calculate the alias-free range (to avoid repeated response):

$$Distance \text{ (one way)} = \frac{V_p * C}{2 * \Delta f}$$

Where V_p is the velocity factor of the transmission line

C is the speed of light

$$\Delta f \text{ (frequency step size)} = \frac{F_{max} - F_{min}}{total \ points - 1}$$

For proper time domain computations, it is always recommended to choose more than adequate frequency points. However, the downside of setting a large number of frequency points is the slower sweep speed.

Time Domain Settings

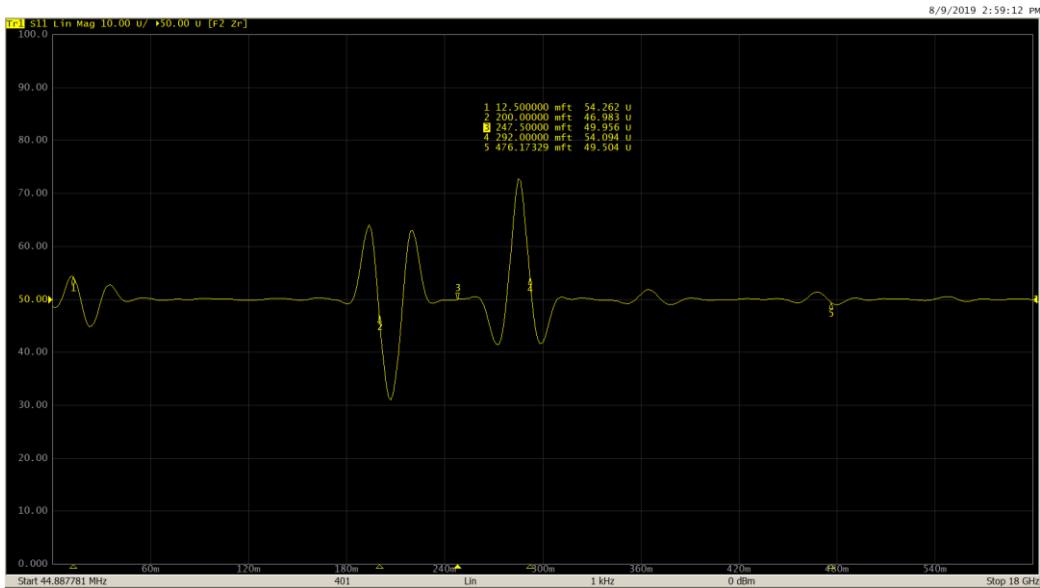
Transformation Type:

A: Bandpass Mode

The bandpass mode is a simpler and generic transformation mode, which simulates the impulse bandpass response. This mode does not require the frequencies to be harmonically related. So, it can be used over any arbitrary frequency range. This is mostly useful for measuring band-limited devices such as filters and waveguides. The disadvantage here is that this mode only allows you to identify locations of mismatches and discontinuities, it does not show if they are capacitive, inductive, or resistive.



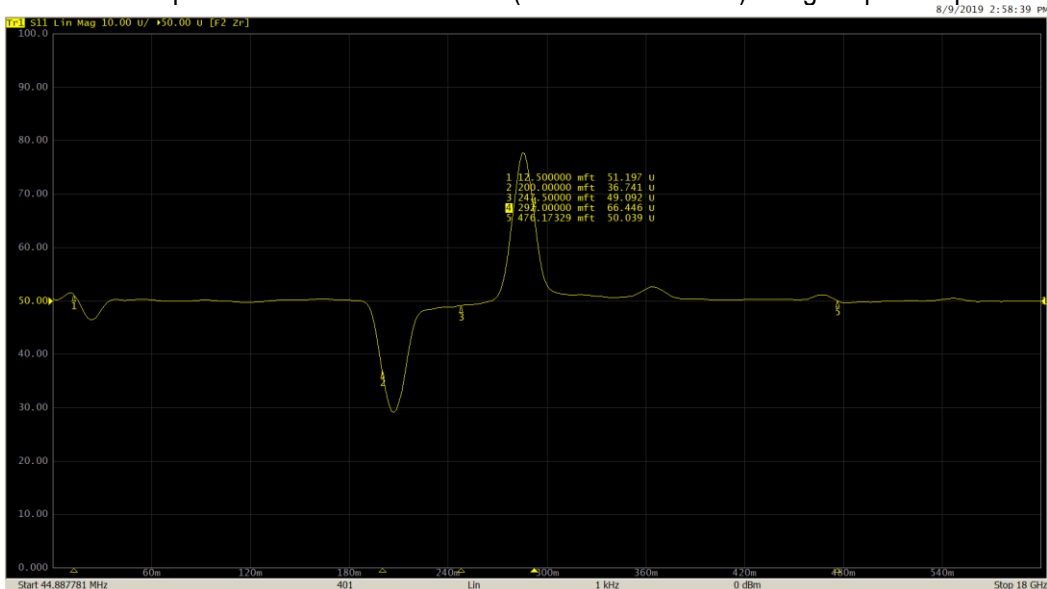
Here is a bandpass mode response for impedance vs. distance on a 50-25-50 Ohm line:



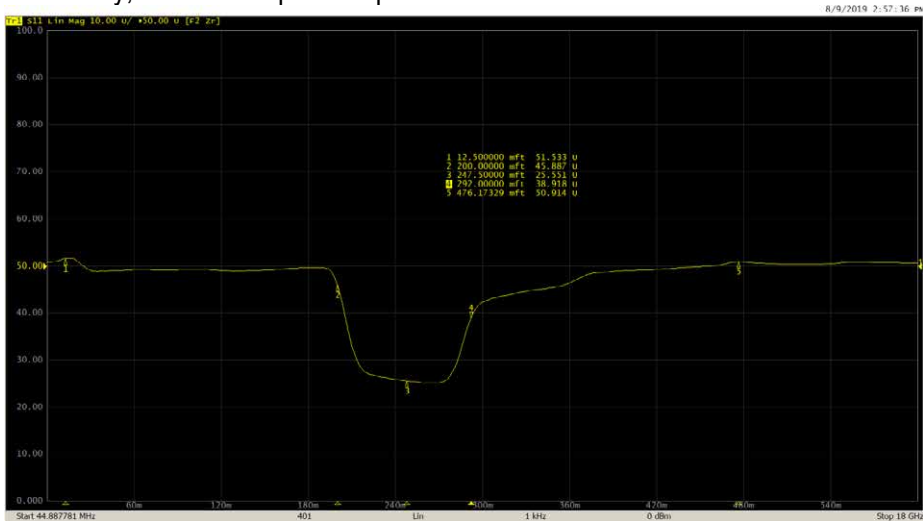
B: Lowpass Mode

The low-pass mode, on the other hand, is useful in determining the type of impedance change present at the mismatch location. This mode simulates lowpass impulse or step responses. In both the low-pass modes, frequencies down to DC are extrapolated to create the harmonic grid necessary for this transformation. Because of this, both step and impulse low-pass modes provide better time domain resolution for a given frequency span than the bandpass mode. In this mode, response to the step and the impulse stimulus contains information describing both, where the mismatch is located, as well as what type of impedance change is present. This mode is suitable for DUTs which go down to DC, such as cables.

Measurement performed on the same DUT (50-25-50 Ohm line) using lowpass impulse mode:



And finally, with the lowpass step mode:



Windowing

In practice, every signal must be finite before processing. So, the input signal must be sampled and truncated before performing time domain transformations. However, this results in spectral leakage at discontinuities. The amount of this leakage is dependent on the amplitude of the discontinuities; which can be adjusted by applying the window function. This is performed by multiplying the time domain signal with a window waveform.

The VNA application uses Kaiser window to perform time domain transformation. The Kaiser window is described by β parameter, which smoothly fine-tunes the window shape from minimum (rectangular) to maximum. The window shape can be fine-tuned or set using the three preprogrammed windows:

- **Minimum** (rectangular);
- **Normal**;
- **Maximum**.

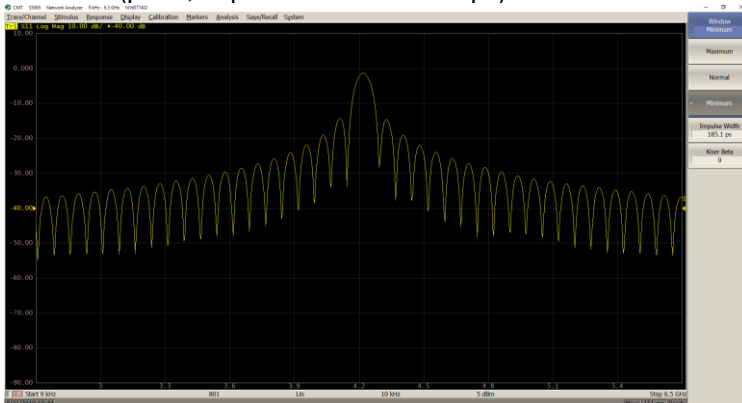
The β values can be adjusted from 0 to 13. 0 corresponds to minimum window, 6 corresponds to normal window, 13 corresponds to maximum window. As the β value increases, it is easy to notice the trade-off between the main-lobe width (or the step rise time in low pass) and the side-lobe level.

| Window | Bandpass Impulse | | Lowpass Impulse | | Lowpass Step | |
|---------|------------------|----------------------------------|------------------|----------------------------------|------------------|----------------------------------|
| | Side Lobes Level | Pulse Width | Side Lobes Level | Pulse Width | Side Lobes Level | Edge Width |
| Minimum | - 13 dB | $\frac{1.2}{F_{max} - F_{min}}$ | - 13 dB | $\frac{0.6}{F_{max} - F_{min}}$ | - 21 dB | $\frac{0.45}{F_{max} - F_{min}}$ |
| Normal | - 44 dB | $\frac{1.96}{F_{max} - F_{min}}$ | - 44 dB | $\frac{0.98}{F_{max} - F_{min}}$ | - 60 dB | $\frac{0.99}{F_{max} - F_{min}}$ |
| Maximum | - 75 dB | $\frac{2.78}{F_{max} - F_{min}}$ | - 75 dB | $\frac{1.39}{F_{max} - F_{min}}$ | - 75 dB | $\frac{1.48}{F_{max} - F_{min}}$ |

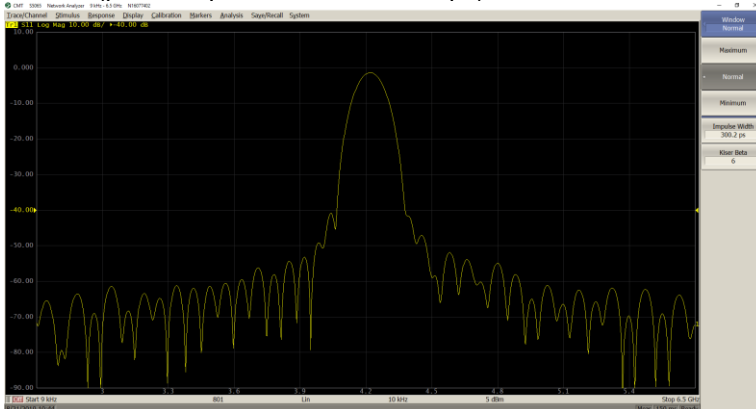
Here are the effects of windowing:

Bandpass Mode:

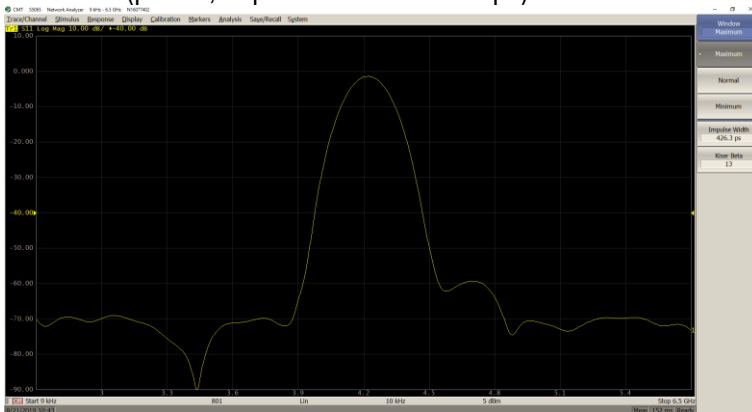
Minimum ($\beta = 0$; Impulse Width = 185.1 ps)



Normal ($\beta = 6$; Impulse Width = 300.2 ps)

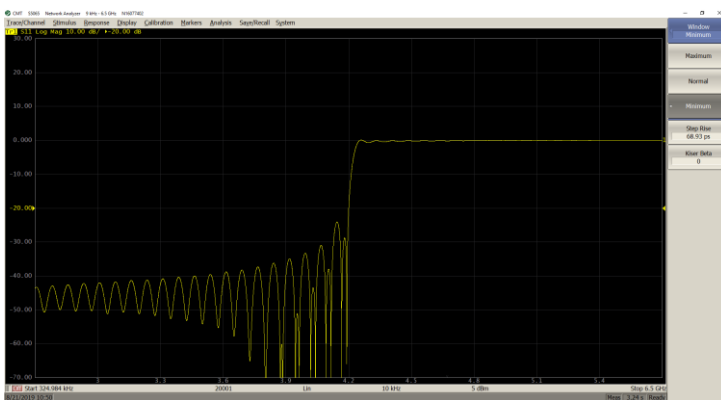


Maximum ($\beta = 13$; Impulse Width = 426.3 ps)

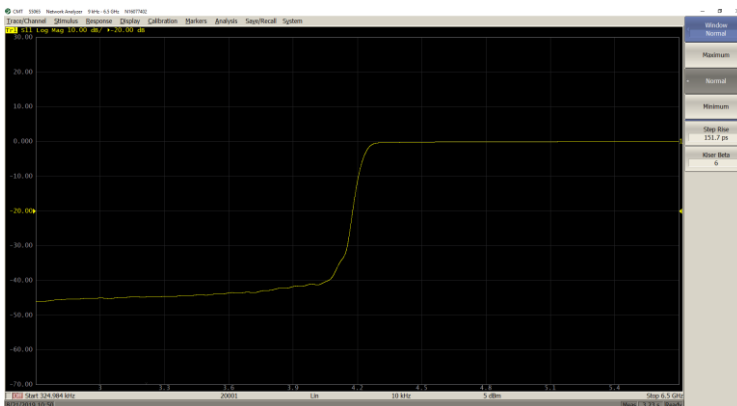


Lowpass step Mode

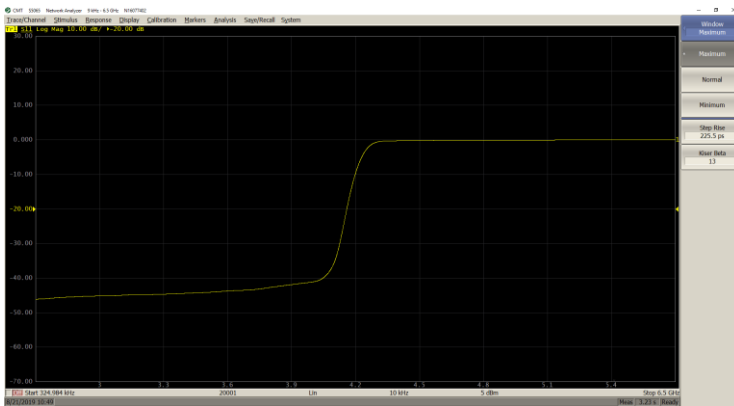
Minimum ($\beta = 0$; Step Rise = 68.93 ps)



Normal ($\beta = 6$; Step Rise = 151.7 ps)



Normal ($\beta = 13$; Step Rise = 225.5 ps)



Velocity Factor

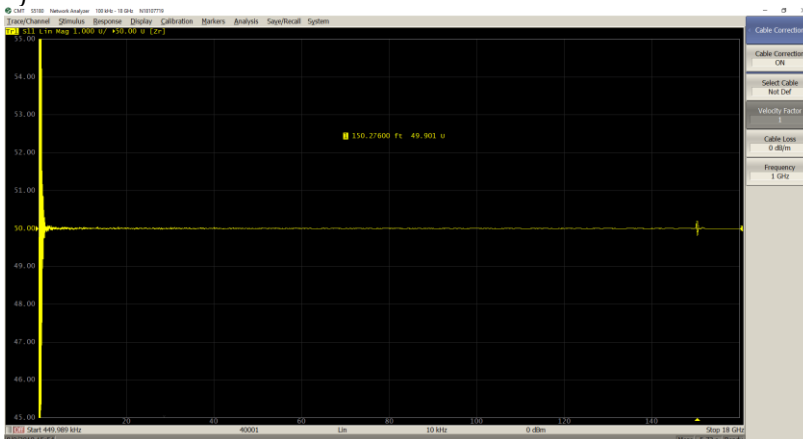
Time and distance are related by velocity. To obtain the accurate mismatch location, it is important to set the right velocity factor of the transmission medium.

By default, the application software assumes it to be equal to 1. But in practice, this can be different depending on the characteristics of the transmission line. If the velocity factor of a transmission line is not known, it can be calculated from the dielectric constant value:

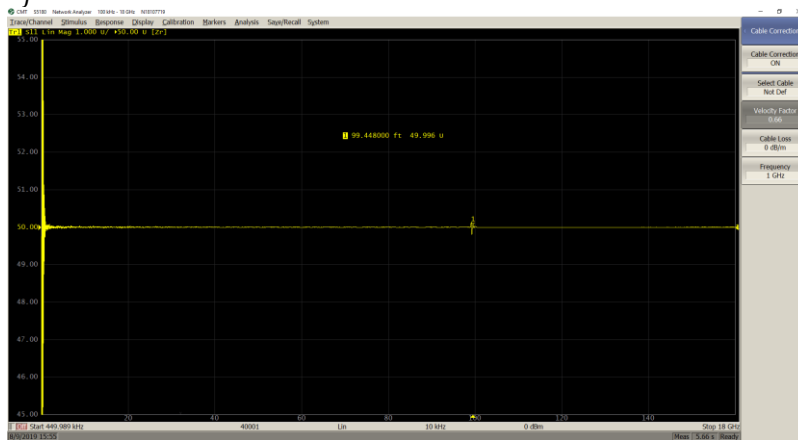
$$V_f = \frac{1}{\sqrt{\epsilon_r}} \quad \text{where } \epsilon_r \text{ is the dielectric constant value}$$

The two measurements below show the impact of entering the proper velocity factor value on a 100 feet cable:

$V_f = 1$



$$V_f = 0.66$$



As seen from the marker values, only by entering the proper velocity factor (0.66 for the cable under test), can the correct length of the cable be seen.

TIME DOMAIN GATING

Time domain gating is another powerful feature in a VNA which mathematically removes the unwanted responses in time domain. The function performs time domain transformation and applies reverse transformation back to frequency domain to the user-defined span in time domain. This function is used to remove the mismatch effects of the fixture devices from the frequency response, if the useful signal and the mismatch signal are separable in time domain.

The function involves two types of time domain gating:

- *bandpass* – removes the response outside the gate span,
- *notch* – removes the response inside the gate span.

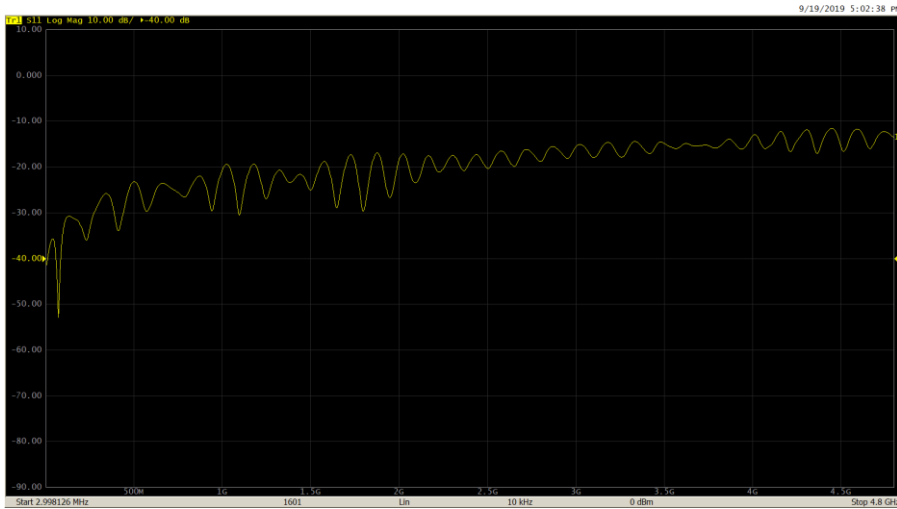
The rectangular window shape in frequency domain leads to spurious sidelobes, due to sharp signal changes at the limits of the window. The following gate shapes are offered to reduce the sidelobes:

- *maximum*;
- *wide*;
- *normal*;
- *minimum*.

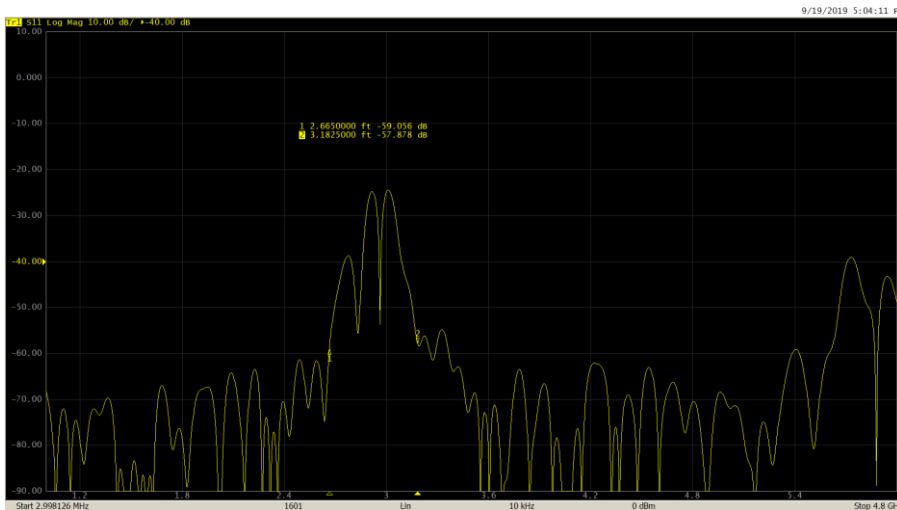
The minimum window has the shape close to rectangular. The maximum window has a more smoothed shape. From minimum to maximum window shape, the sidelobe level increases and the gate resolution reduces. The choice of the window shape is always a trade-off between the gate resolution and the level of spurious sidelobes.

Here is the effect of applying gating on a mismatch in a 50 Ohm cable:

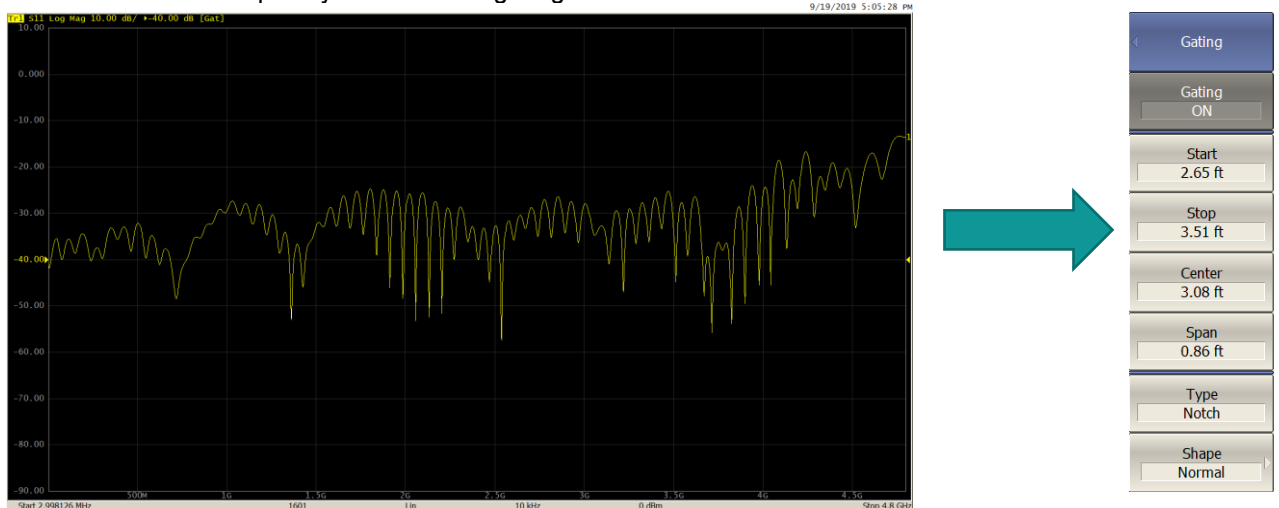
S11 return loss in frequency domain before applying gating:



Response viewed in time domain:



S11 return loss in frequency domain after gating:



After gating out the mismatch using 'Notch' type, as expected, the S11 return loss shows improvement.

ACCURACY CONSIDERATIONS

Due to the intricacies involved in setting up time domain measurements for various applications, the measurement accuracy of a vector network analyzer (VNA) in time domain is not specified. Therefore, these data are not stated in the specifications, since they depend not only on the parameters of the VNA in the frequency domain, but also on the properties and configuration of the device under test (DUT) in the time domain.

Measurement of delay (or distance) primarily depends on two factors:

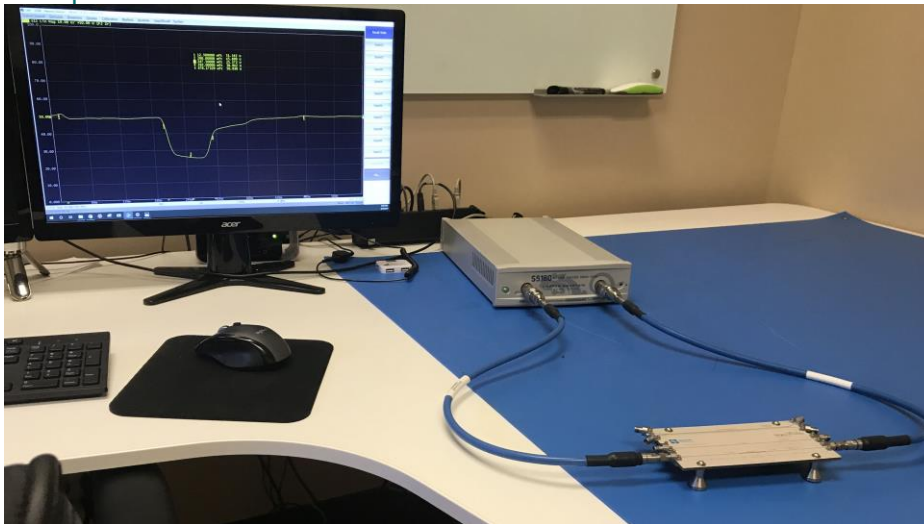
First, the frequency span or the maximum frequency of the VNA determines the resolution in time domain (inversely proportional as mentioned above in the 'Calculator' section). Based on the transformation setting, the maximum error can be equal to half the resolution:

$$\Delta \tau_{\text{max}} = \frac{1}{2f_{\text{max}}} \text{ (band-pass mode)} \quad \Delta \tau_{\text{max}} = \frac{1}{4f_{\text{max}}} \text{ (low-pass mode)}$$

Secondly, when the delay is recalculated into distance considering the value of the effective permittivity of the medium. The error in known permittivity increases the error in calculating the distance.

COMMON APPLICATIONS

A: Impedance on a PCB line



Setup

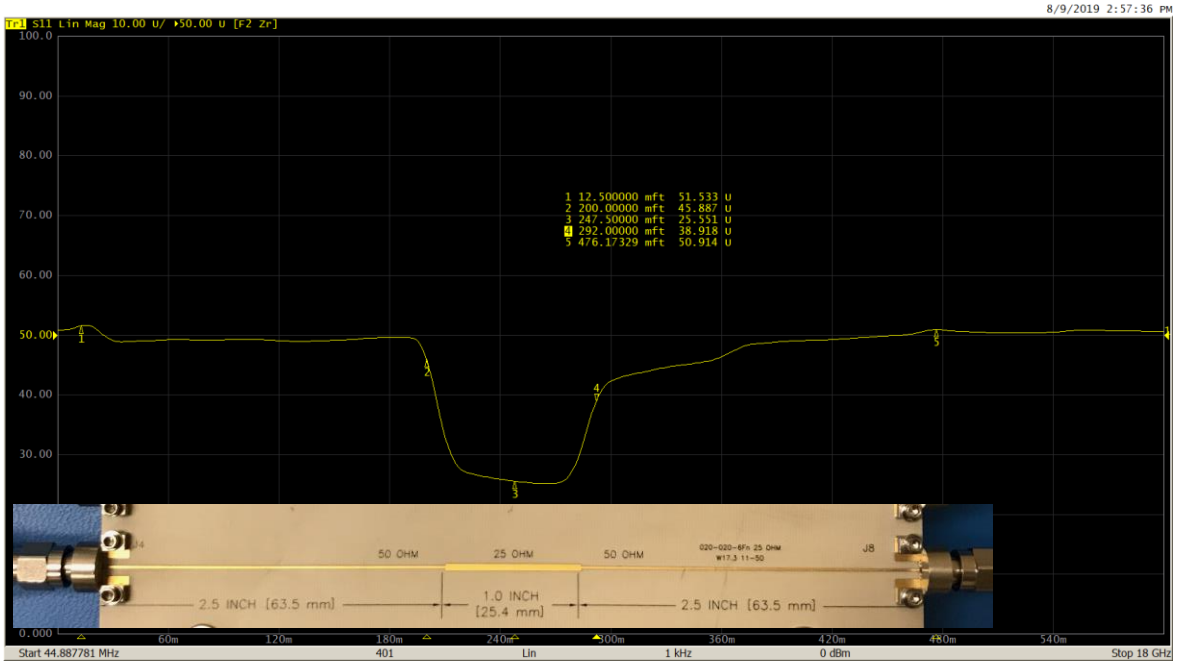
S5180 VNA (2-port, 100 kHz to 18 GHz), two N-type to 3.5 mm adapters, two 2.92 mm coaxial cables and a sample board with a 25 Ohm Beatty line.

Steps

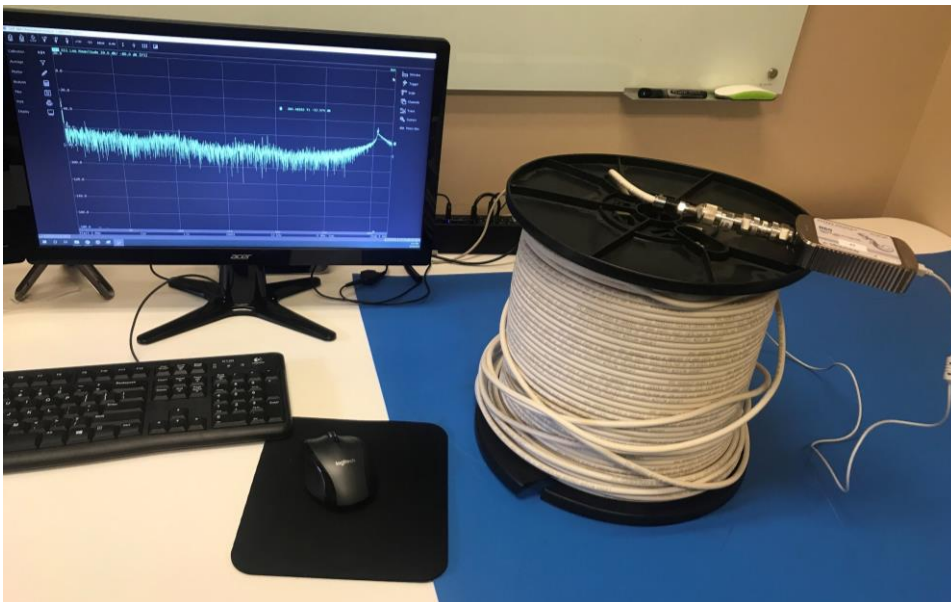
- 1) Set the stimulus settings: frequency span, points, and linear sweep type.
- 2) Click 'Set Frequency Low Pass' to create a harmonic grid (*Analysis > Time Domain > Set Frequency Low Pass*).
- 3) Perform full 2-port calibration at the measurement plane (*Calibration > Calibrate*).
- 4) Adjust time domain settings (*Analysis > Time Domain*): unit, reflection type – one way, velocity factor and loss, start and stop value, transformation type – Lowpass step, Window – Normal.
- 5) Enable time domain mode (*Analysis > Time Domain > ON*).
- 6) Adjust the display settings to measure impedance (y-axis) vs. distance (x-axis):
 - a) Set trace to 'S11 linear magnitude'.
 - b) Enable impedance measurement (*Analysis > Conversion > Function – Z:Reflection > ON*).



Measurement



B: DTF on a long cable

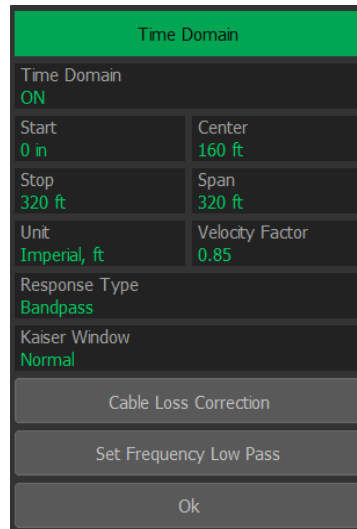


Setup

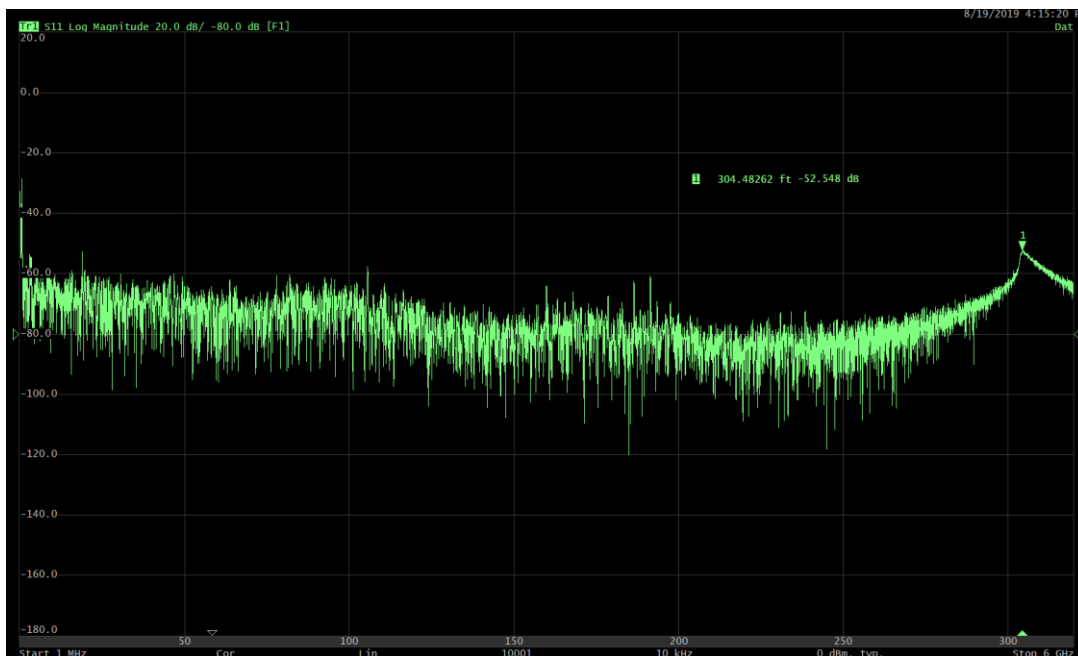
R60 VNA (1-port, 1 MHz to 6 GHz), one N-type 50 Ohm barrel, one N-type 50 Ohm to 75 Ohm adapter, one N-type to F-type adapter, one 300-foot-long CATV cable under test.

Steps

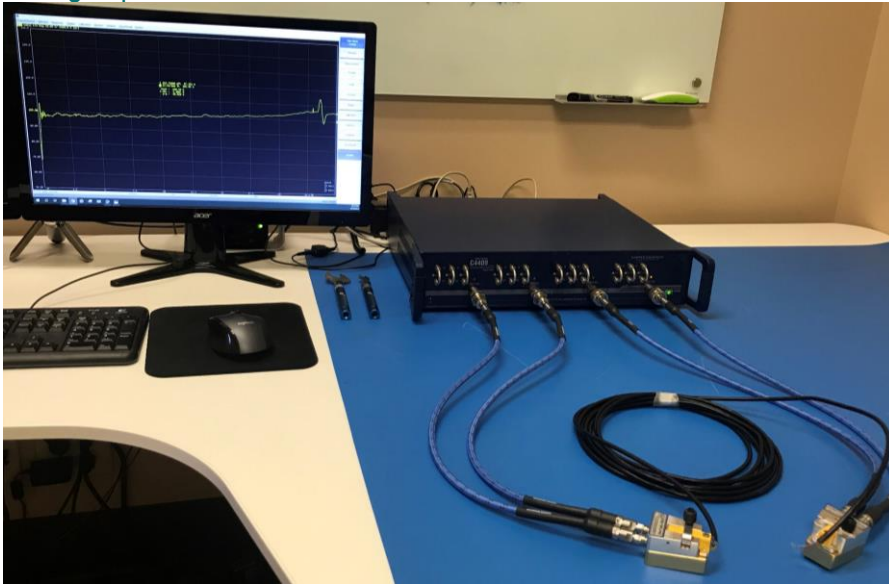
- 1) Set stimulus settings: frequency span, points, and linear sweep type.
- 2) Perform full 1-port calibration at the end of the measurement plane (*Calibration > Calibrate*).
- 3) Adjust time domain settings (*Analysis > Time Domain*): unit, reflection type – one way, velocity factor and loss, start and stop value, response type – Bandpass, Window – Normal.
- 4) Enable time domain mode (*Analysis > Time Domain > ON*).
- 5) Adjust the display settings to measure return loss (y-axis) vs distance (x-axis) (Trace > Format – Log Magnitude)



Measurement



C: High speed differential measurements



Setup

C4409 VNA (4-port, 100 kHz to 9 GHz), four N-type to 3.5 mm adapters, four 2.92 mm coaxial cables, two coaxial to raw cable fixtures and a 100 Ohm differential high speed LVDS cable under test.

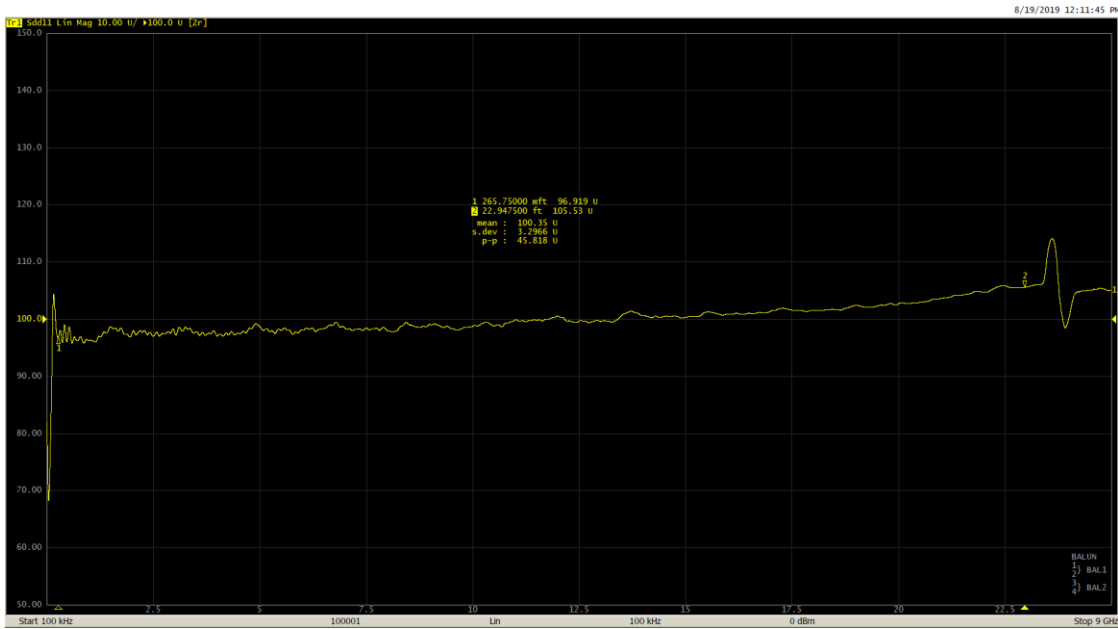
Steps

- 1) Set stimulus settings: frequency span, points, and linear sweep type.
- 2) Click 'Set Frequency Low Pass' to create a harmonic grid (*Analysis > Time Domain > Set Frequency Low Pass*).
- 3) Perform full 4-port calibration at the end of the coaxial cables (*Calibration > Calibrate*).
- 4) De-embed the fixtures using the touchstone files provided by the manufacturer (*Analysis > Fixture Simulator > De-Embedding s4p*).
- 5) Enable balanced mode to measure the differential parameter Sdd11 (*Analysis > Fixture Simulator - ON > BalUn - ON*)
- 6) Adjust the time domain settings (*Analysis > Time Domain*): unit, reflection type – one way, velocity factor and loss, start and stop value, transformation type – Lowpass step, Window – Normal.
- 7) Enable time domain mode (*Analysis > Time Domain > ON*).

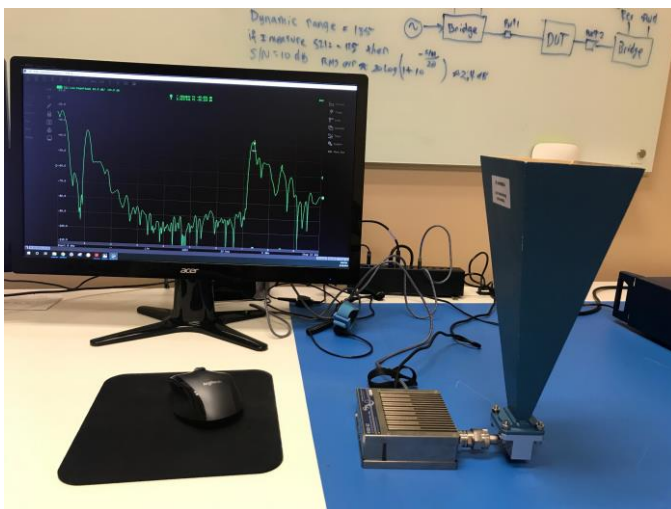


- 8) Adjust the display settings to measure impedance (y-axis) vs distance (x-axis):
 - a) Set trace to 'Sdd11 linear magnitude'.
 - b) Enable impedance measurement (*Analysis > Conversion > Function – Z:Refletion > ON*).

Measurement



D: X-band horn antenna

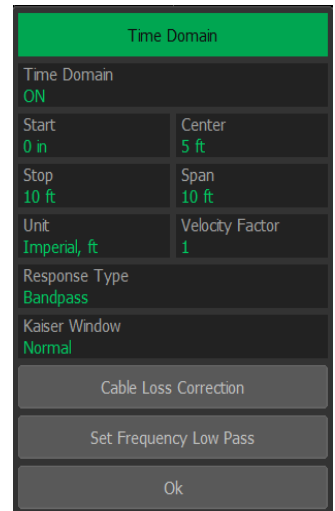


Setup

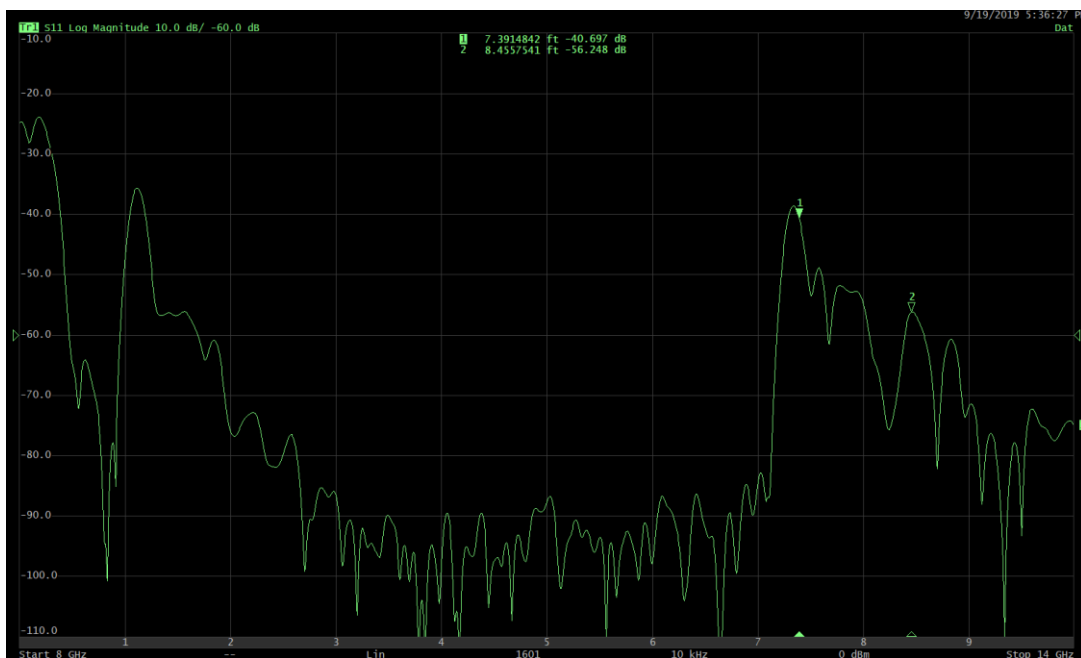
R180 VNA (1-port, 1 MHz to 18 GHz) and X-band antenna

Steps

- 1) Set stimulus settings: frequency span, points and linear sweep type.
- 2) Perform full 1-port calibration at the end of the measurement plane (*Calibration > Calibrate*).
- 3) Adjust time domain settings (*Analysis > Time Domain*): unit, reflection type – one way, velocity factor and loss, start and stop value, response type – Bandpass, Window – Normal.
- 4) Enable time domain mode (*Analysis > Time Domain > ON*).
- 5) Adjust the display settings to measure return loss (y-axis) vs distance (x-axis) (*Trace > Format – Log Magnitude*)



Measurement



CONCLUSION

As a VNA measures both the magnitude and the phase of the DUT in frequency domain, we have seen that using the built-in inverse Fourier transformation algorithm measurements could be viewed in the time domain mode as well. We have seen how different settings can impact the time domain transformation, and the various applications that could be performed using this feature.

If you need further information on this application note or any assistance with your application, please contact: support@coppermountaintech.com.

REFERENCES

- 1) "The Chirp z-Transform Algorithm", *L. R. Rabiner, R. W. Shafer, C. M. Rader*
- 2) "S2VNA Operating Manual" <https://coppermountaintech.com/s2-operating-manual/>
- 3) "Time Domain Reflectometry Measurements with a Vector Network Analyzer" video <https://coppermountaintech.com/video-time-domain-reflectometry-measurements-with-a-vector-network-analyzer/>, *Brian Walker*
- 4) "Sparse Inverse Chirp-Z Transform of S-Parameter Measurements for Time Domain Analysis of Transmission Line", *Guilherme H. Weber, Hector L. Moura, Guilherme Dutra, Uilian J. Dreyer, Rafael J. Daciuk, Jean C. C. da Silva, Cicero Martelli, Daniel R. Pipa, Marco J. da Silva.*
- 5) "Time-Domain Reflectometry using S-Parameters and De-embedding Application", *A. S. Ali and R. Mittra*
- 6) "Fundamentals of Vector Network Analysis", *Michael Hiebel*



Characterizing Uncertainty in S-Parameter Measurements

Tekamul Buber, Pragti Narang, Giampiero Esposito and Sathya Padmanabhan
Maury Microwave, Ontario, Calif.

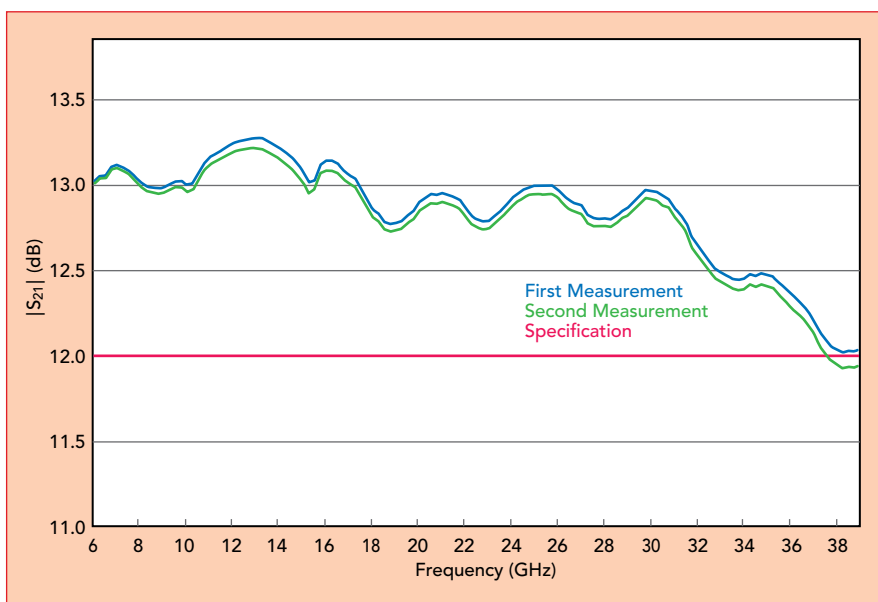
Markus Zeier
Federal Institute of Metrology (METAS), Berne-Wabern, Switzerland

One might ask why engineers should expand their S-parameter measurement practices to include uncertainties, since they have been largely ignored until now. The answer lies mainly in the advancement of technology: as new technologies emerge and are introduced as standards, the specifications and requirements for products get tighter, especially with increasing frequency. This trend can be seen not only with systems, but also at the component level, including amplifiers, filters and directional couplers. Therefore, engineers responsible for the design and production of these components need to increase the confidence in their measurements and product characterization.

Imagine the following: an engineer designs an amplifier requiring a minimum gain over a frequency bandwidth. The amplifier is measured and meets the specification. A few hours later, the amplifier is remeasured and no longer meets the specifications at the high end of the frequency band (see **Figure 1**). Why is the amplifier not meeting the specification? There could be many reasons: the measurement system drifted, someone in the lab moved or damaged one of the cables in the measurement setup or one of many other possibilities, including doubts about the design, fabrication or stability of the product.

If it is that easy to take two measurements and obtain different results, how can one know which measurement is

correct? The confusion arises from not characterizing and including the uncertainties in the measurement, which ultimately leads to an overall lack of confidence in the results. Careful engineers use methods to validate a setup before taking measurements. More careful users test “golden devices”—those with similar characteristics to the actual device under test (DUT)—as a validation step and reference internal guidelines to decide whether the data is good enough. While this is a step in the right direction, how are these guidelines defined? Are the guidelines truly objective, or is subjectivity built in? How close is close enough? Uncertainty evaluation is a powerful tool allowing users to both validate vector network analyzer (VNA) calibration and properly define metrics for golden devices before taking measurements. **Figure 2** illustrates this,



▲ Fig. 1 Amplifier gain measurements at two times: the first in spec, the second out of spec at the upper band edge.

showing the same amplifier gain measurement with the uncertainties of the system.

UNCERTAINTIES

Every measurement, no matter how carefully performed, inherently involves errors. These arise from imperfections in the instruments, in the measurement process, or both. The “true value of a measured quantity” (a_{true}) can never be known and exists only as a theoretical concept. The value that is measured is referred to as “indication” or (a_{ind}), and the difference between the true value and the measurement indication is the error:

$$e = a_{\text{true}} - a_{\text{ind}} \quad (1)$$

Since the true value is unknown, the exact error e in the measurement is also unknown. There are two types of errors:

Systematic errors: In replicate measurements, this component remains constant or varies in a systematic manner and can be modeled, measured, estimated and, if possible, corrected to some degree.¹ Remaining systematic errors are unknown and need to be accounted for by the uncertainties.

Random errors: This component varies in an unpredictable manner in replicate measurements.² Some examples are fluctuations in the measurement setup from temperature change, noise or random effects of the

operator. While it might be possible to reduce random errors—with better control of the measurement conditions, for example—they cannot be corrected for. However, their size can be estimated by statistical analysis of repetitive measurements. Uncertainties can be assigned from the results of the statistical analysis.

In general, a measurement is affected by a combination of random and systematic errors; for a proper uncertainty evaluation, the different contributions need to be characterized. A measurement model is needed to put the individual influencing factors in relation with the measurement result.³ Coming up with a measurement model that approximates reality sufficiently well is usually the hardest part in uncertainty evaluation. Propagating the uncertainties through the measurement model to obtain a result is merely a technical task, although sometimes quite elaborate. Finally, the measurement result is generally expressed as a single quantity or estimate of a measurand (i.e., a numerical value with a unit) and an associated measurement uncertainty u . This procedure, described here, is promoted by the “Guide to the expression of uncertainty in measurement” (GUM),⁴ which is the authoritative guideline to evaluate measurement uncertainties.

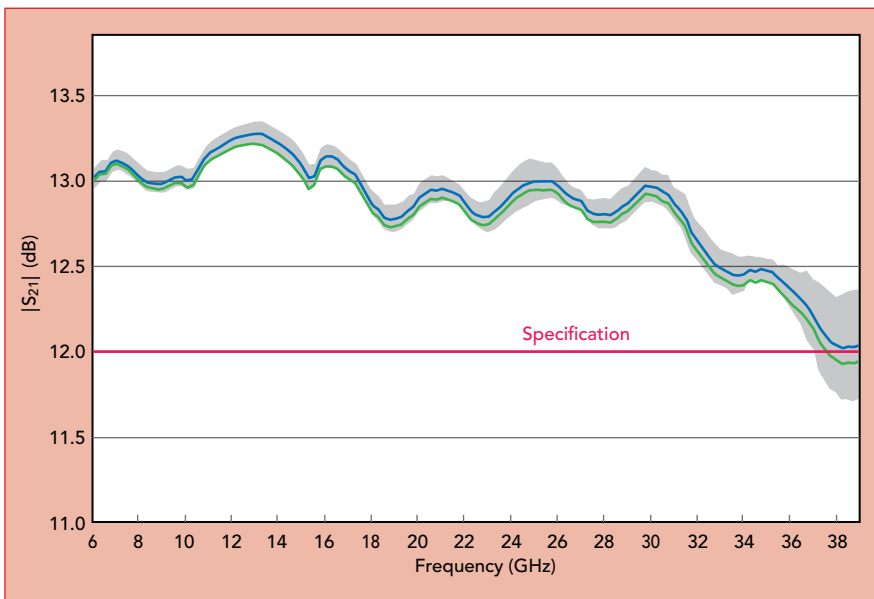
S-PARAMETERS AND VNA CALIBRATION

How do these concepts apply to S-parameter measurements? Recall that S-parameters are ratios of the incident (pseudo) waves, denoted by a , and reflected (pseudo) waves, denoted by b :

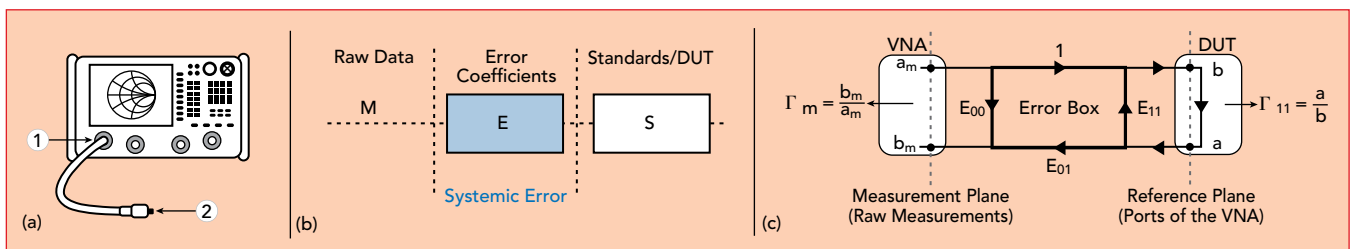
$$S_{11} = \frac{b_1}{a_1}, S_{21} = \frac{b_2}{a_1} \quad (2)$$

The definition of S-parameters implies a definition of reference impedance.⁵⁻⁶ The most common measurement tool used to measure S-parameters is a VNA. While different VNA architectures exist, the most common versions for two-port measurements use either three or four receivers.⁵⁻⁷

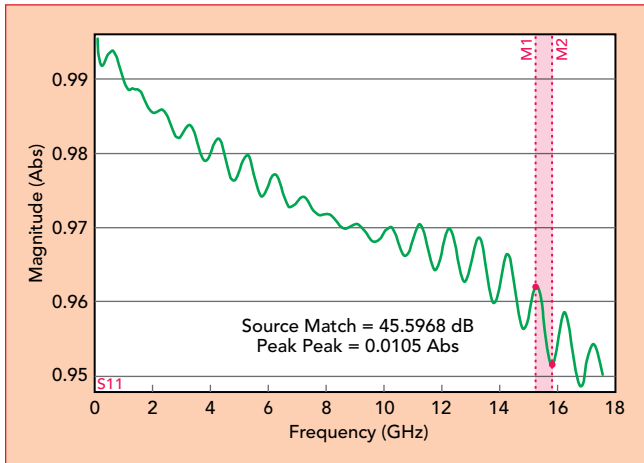
To simplify the understanding of the subject, consider a one-port VNA measurement (see **Figure 3**). The case for two-port or more general N-port measurements can be obtained through generalizations, as shown in the literature.⁷ Figure 3a shows a typical setup, where a VNA, cable and



▲ Fig. 2 Amplifier gain measurement showing measurement uncertainty, calculated using Maury MW Insight software.



▲ Fig. 3 One-port measurement hardware setup (a), systemic error model (b) and signal flow graph (c).



▲ Fig. 4 Source match after one-port calibration using Maury MW Insight software.

connectors are used as a measurement system to measure a DUT. To evaluate uncertainties in the S-parameter measurements, a measurement model first needs to be established, to describe the relation between the output variables, the incident and reflected waves at a well-defined port (i.e., the reference plane), and the indications at the VNA display (i.e., the raw voltage readings of the VNA receivers). These models should include systematic as well as random errors to increase confidence in the results. Not estimating systematic errors correctly leads to inaccurate measurements. On the other hand, wrong estimates of the random errors can either degrade the precision of the result or indicate the results are precise when they are not.

CLASSICAL VNA ERROR MODEL

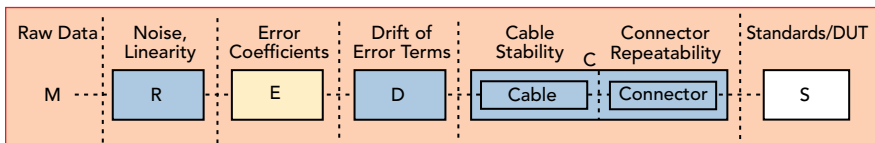
VNA measurements are affected by large systematic errors which are unavoidable and inherent to the measurement technique, related to signal loss and leakage. They establish a relation between the indication (measured)

$$\Gamma_m = \frac{b_m}{a_m}$$

and the S-parameter at the reference plane

$$\Gamma_{11} = \frac{b}{a}$$

shown by the signal flow graph of Figure 3c. The error box consists of three error coefficients: directivity (E00), source match (E11) and reflection tracking (E01). The graphical representation in Figure 3b can be transformed into a bilinear function between the indications and S-parameters at the reference plane through the three unknown error coefficients. To estimate the unknown error coefficients of the model, three known calibration standards must be measured for the one-port case, more if multiple ports are involved. After estimat-



▲ Fig. 5 VNA measurement model.

ing the error coefficients, any subsequent measurement of raw data (i.e., indications) can be corrected. This technique is commonly referred to as VNA calibration and VNA error correction.

Different calibration techniques have been developed to estimate the error coefficients. Some require full characterization of the calibration standards, such as short-open-load (SOL) or short-open-load-thru (SOLT), while others require only partial characterization, such as thru-line-reflect (TRL), short-open-load-reciprocal thru (SOLR) and line-reflect-match (LRM) for two-port calibrations.⁸ Even if the calibration standards are characterized, they are not perfectly characterized, and the error associated with the characterization will increase the inaccuracy of the estimated error coefficients: directivity, source match and reflection tracking.

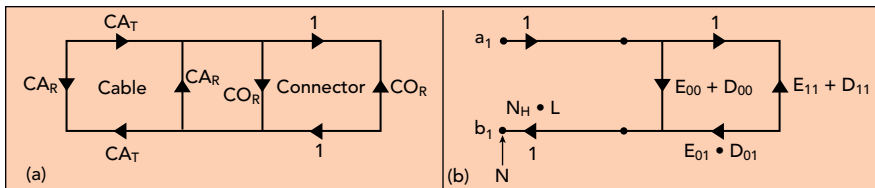
Engineers have developed experimental techniques to estimate these residual errors (i.e., residual directivity, residual source match and residual reflection tracking). Connecting a beadless airline terminated with a reflection standard to the calibrated port enables the residual errors to be observed as a superposition of reflections versus frequency. In the frequency domain, this implies ripples in the reflection coefficient (see Figure 4). Due to the characteristic pattern in the frequency response, the method is referred to as the “ripple method,” where the magnitude of the ripples is used to estimate the residual errors and uncertainties related to directivity and source match. This method has various shortcomings: it is unable to determine the residual error in tracking and requires handling air-dielectric lines, which becomes impractical as frequency increases.⁷

Residual errors have been used to gain confidence in the measurement based on experience. The challenge is to understand what a residual directivity of 45 dB means if a DUT with 36 dB return loss is measured. However, the uncertainties of the error coefficients are not reliable when estimated with the ripple method, and they are insufficient to gain confidence in the measurement results. The classical VNA error model is thus incomplete to perform VNA calibration and VNA error correction with uncertainty evaluation.

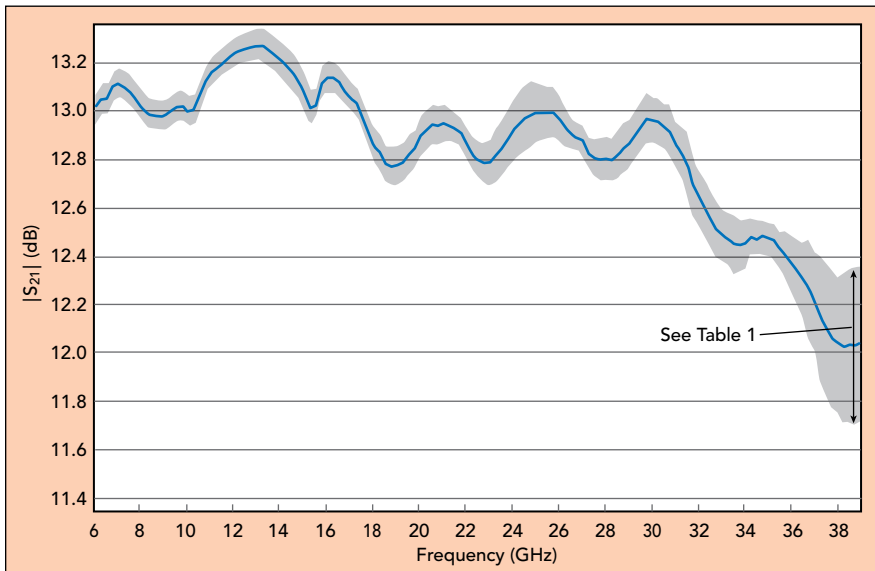
ADDING UNCERTAINTIES TO THE CLASSICAL VNA ERROR MODEL

This section explains how to expand the classical VNA error model into a full measurement model by adding the other factors influencing the measurement. Using such a full model, the uncertainties can be evaluated in a direct and conceptually clear method. The measurement setup leading from the calibration reference plane to the receiver indications contains several sources of error and influence factors that contribute to the total uncertainty. The classical VNA error model can be expanded to include these factors, becoming a full measurement model. Typical components include the VNA (e.g.,

linearity, noise and drift), cables, connectors and the calibration standards. The European Association of National Metrology (EURAMET) recommends the model shown in Figure 5, where the traditional error coefficients are



▲ Fig. 6 Models for the cable and connector (a) and VNA noise, linearity and drift (b).



▲ Fig. 7 Total amplifier gain measurement uncertainty, calculated using Maury MW Insight software.

identified by the E block and the other influence factors represented by the R, D and C blocks.^{7,9} The full model in the figure contains just the building blocks, which are further refined using signal flow graphs. Without going into the details of these models, the main errors and related signal flow graphs are described.

Cable and Connector

Cables are used between the reference plane and the receiver indications, making them part of the calibration. They are subject to environmental variations, as well as movement and bending. When cables are moved or bent during calibration or DUT measurement, the error coefficients are expected to change. The cable model uses two parameters: cable transmission (CA_T) and cable reflection (CA_R), shown in **Figure 6a**. While cable suppliers typically specify these values in cable assembly datasheets, the cables should be characterized for the typical range of flexure or movement during calibration and measurement.⁷

Similarly, the connectors used for connecting and disconnecting the calibration standards and DUT affect the reference plane, based on how repeatable the pins and fingers are designed and built. The S-parameter response of a device differs each time it is connected, disconnected and reconnected, which is modeled by one parameter, the connector repeatability (CO_R).

VNA

The receivers in the VNA tend to deviate from linear behavior at high input power levels. Nonlinearity is essentially a systematic error that can be corrected using

an appropriate nonlinear model. Since the nonlinear behavior may be different for each receiver and modeling each is impractical, the non-linearity is approximated with a linear model, denoted as L in **Figure 6b**.

Noise is a random error and encompasses unpredictable fluctuations in the indications of the VNA. The noise influence is divided into the noise floor (N_L) and trace noise (N_H), where the noise floor is observed without any source signal, and the trace noise scales with the applied source signal level.

Drift accounts for changes in the performance of the entire measurement system over time, due to thermal and other environmental effects. A simple model associates a drift value (D_{00} , D_{11} , D_{01}) to each error term, as shown in **Figure 6b**.

Calibration Standards

The calibration standards need to be characterized, including their associated uncertainties (shown as block S in **Figure 5**). Depending on the level of accuracy required, this can be obtained from the manufacturer, a calibration laboratory or a national metrology institute, with the characterization traceable to SI units.¹⁰ It has been demonstrated that coaxial calibration standards can be characterized more accurately and more consistently by including the effects of the connectors in the characterization.¹¹ When performing the VNA calibration to estimate the error coefficients, these uncertainties are propagated together with the other contributions to the error coefficients.

Once all the sources of error and influences are modeled and estimated, VNA calibration and error correction can be performed. Uncertainty contributions are propagated through the full measurement model to the measurement results. This will be sufficient to have confidence in the measurement if the following conditions are met:

- All sources of significant errors and influences are included in the models (see the error models described previously).
- The sources are estimated realistically, i.e., these errors are characterized based on the real measurement conditions; in some cases, supplier specifications may not be sufficient.
- The calibration standards are characterized accurately with realistic uncertainties.

The first condition is usually satisfied for most measurement setups. The second depends mostly on the operator estimating the uncertainties, and the third depends on the source characterizing the standards.

Using this approach will enable engineers to determine an uncertainty budget and the major contributions

to the overall uncertainty. This is a powerful tool because it shows where to improve system accuracy if the uncertainty is too high. To illustrate, in the amplifier measurement (see **Figure 7** and **Table 1**), cable stability and connector repeatability represent more than 90 percent of the total uncertainty.

VERIFICATION AND VALIDATION TOOL

Several methods and techniques are used to validate a calibration. Some use T-checkers or Beatty standards, others use pre-characterized verification standards. The quality of a calibration can be “bad” due to sources of error, such as mixing standards, damaged standards and cables, loose connections or sudden noise in the system due to environmental changes. Since these significant sources of error are usually not accounted for in the characterization of the uncertainty contributors, they will not be considered in the uncertainty budget, which will degrade the quality of the calibration and, hence, measurement accuracy.

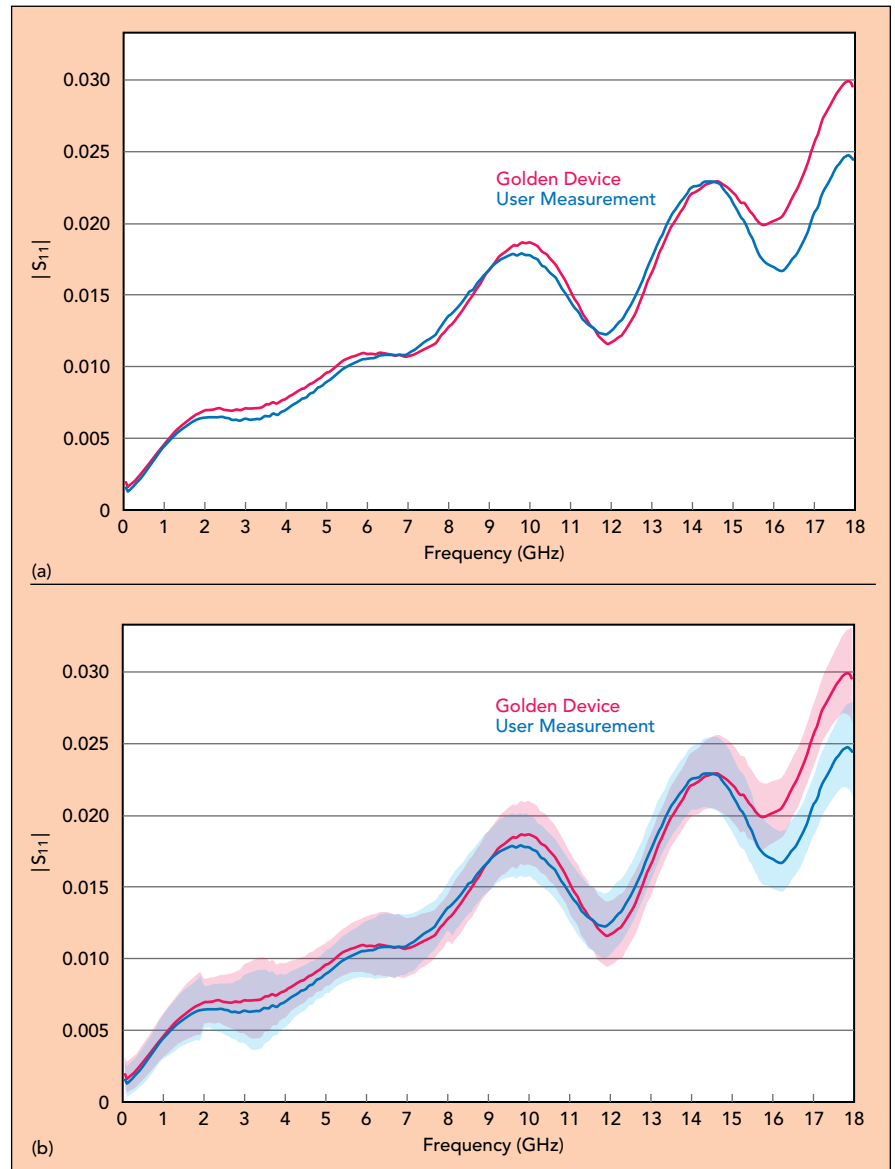
This section addresses verification devices, because they enable the validation of the calibration accuracy and estimate the level of precision achievable. Verification per the International Vocabulary of Metrology (VIM) definition¹² provides objective evidence that the calibration fulfills specified requirements; however, as these requirements can be specified quite arbitrarily, more important than the verification is the validation¹³, which is the verification whose specified requirements are adequate for measuring the devices intended for measurement.

Most of the current verification devices are not characterized with

uncertainties, and it is difficult for the user to specify an adequate requirement for the validation. In most cases, the user compares the reference characterization with the actual measurement and estimates how close the two are. This is quite subjective, as shown in **Figure 8a**, which shows a difference in magnitude; the question is whether this is sufficient. Had the results included uncertainties, the user could proceed more systematically and quantitatively as follows:

- Choose a verification standard which has been previously characterized with uncertainties and is representative of the measurement. For example, a fixed load different than one used as a calibration standard can be selected for a one-port, low reflection measurement.
- Validate that the uncertainties of the setup are not too large by 1) comparing the setup uncertainty with the uncertainty provided by the manufacturer of the verification device; 2) comparing the setup uncertainty

| Source | Magnitude (x 10 ⁻³) | Percentage (%) |
|----------------------|---------------------------------|----------------|
| VNA Noise Floor | 1.145 | 0.104 |
| VNA Noise Trace | 4.520 | 1.615 |
| VNA Linearity | 7.163 | 4.056 |
| VNA Drift Tracking | 0.5132 | 0.021 |
| VNA Drift Symmetry | 0.5444 | 0.023 |
| Cable Transmission | 33.26 | 87.47 |
| Cable Reflection | 8.630 | 5.887 |
| Connector Reflection | 3.227 | 0.823 |



▲ Fig. 8 Comparison of “golden” device and user measurements (a); same data showing measurement uncertainty (b).

ty at the 95 percent confidence level with the design tolerance of the DUT. The expanded uncertainty for the 95 percent confidence interval should always be smaller than the design tolerance; and 3) if the uncertainties do not satisfy the above two conditions, re-evaluate the VNA, cable, connector and the calibration kit used for the calibration.

- A normalized error can be used to finalize the validation,⁷ where the scalar version is defined by:

$$e = \frac{1}{1.96} \frac{|\hat{d}|}{u(\hat{d})} \quad (3)$$

Where \hat{d} is the estimate of the difference between the measurement and verification device and $u(\hat{d})$ is the estimate of the standard uncertainty of the difference. The factor 1.96 corresponds to a 95 percent coverage condition, which is quite common in conformity assessment. **Figure 8b** shows the uncertainties of the same amplifier measurement from Figure 8a. Areas of insufficient overlap of the two uncertainties result in values of $e > 1$ and indicate a failed verification.

CONCLUSION

As technologies evolve and requirements become more challenging, implementing processes that increase confidence in measurements and ensure accurate and reliable characterization—and product performance—are critical. Characterizing and quantifying measurement uncertainty is one such process to achieve the desired results. Uncertainty can aid in definitively verifying a VNA calibration before measuring a DUT. Uncertainty can help understanding how the various components in a measurement system impact the overall uncertainty of the DUT measurement. Identifying, quantifying and reducing the major sources of uncertainty in a test setup will improve the accuracy of the overall measurement. Referring to the original amplifier scenario shown in Figure 1, quantifying measurement uncertainty can provide

the confidence that the true performance of the DUT is reflected in the measurements, and the design will not pass one test and fail another. ■

References

1. Clause 2.17, "VIM: International Vocabulary of Metrology, Third Edition," *JCGM 200:2012*, www.bipm.org/en/publications/guides/vim.html.
2. Clause 2.19, "VIM: International Vocabulary of Metrology, Third Edition," *JCGM 200:2012*, www.bipm.org/en/publications/guides/vim.html.
3. Clause 2.48, "VIM: International Vocabulary of Metrology, Third Edition," *JCGM 200:2012*, www.bipm.org/en/publications/guides/vim.html.
4. Evaluation of Measurement Data, "Guide to the Expression of Uncertainty in Measurement," *JCGM 100:2008*, www.bipm.org/en/publications/guides/gum.html.
5. M. Hiebel, "Fundamentals of Vector Network Analysis," *Rohde & Schwarz*, 2007.
6. J. P. Dunsmore, "Handbook of Microwave Component Measurements," 2014.
7. M. Zeier, D. Allal and R. Judaschke, "Guidelines on the Evaluation of Vector Network Analyzers (VNA), *EURAMET Calibration Guide*, No. 12, Version 3, 2018, www.euramet.org/publications-media-centre/calibration-guidelines/.
8. "Improving Calibration Accuracy and Speed with Characterized Calibration Standards," *Maury Microwave App Note 5C-090*.
9. M. Zeier, J. Hoffmann, J. Ruefenacht and M. Wollensack, "Contemporary Evaluation of Measurement Uncertainties in Vector Network Analysis," *Cal Lab Magazine*, October–December 2018, pp. 22–31, www.callabmag.com/contemporary-evaluation-of-measurement-uncertainties-in-vector-network-analysis/.
10. Clause 2.41, "VIM: International Vocabulary of Metrology, Third Edition," *JCGM 200:2012*, www.bipm.org/en/publications/guides/vim.html.
11. M. Zeier, J. Hoffmann, P. Hürlimann, J. Rüfenacht, D. Stalder and M. Wollensack, "Establishing Traceability for the Measurement of Scattering Parameters in Coaxial Line Systems," *Metrologia* 55, January 2018, S23–S36.
12. Clause 2.44, "VIM: International Vocabulary of Metrology, Third Edition," *JCGM 200:2012*, www.bipm.org/en/publications/guides/vim.html.
13. Clause 2.45, "VIM: International Vocabulary of Metrology, Third Edition," *JCGM 200:2012*, www.bipm.org/en/publications/guides/vim.html.

S5065 and S5085



The 2-port 6.5 or 8.5 GHz VNAs deliver lab-grade performance in a compact package, with all the features engineers have come to expect included standard in our Windows or Linux software. These portable VNAs can be battery powered and used for field, laboratory, and production testing.

LEARN MORE



Using a VNA for Power Plane Impedance Analysis

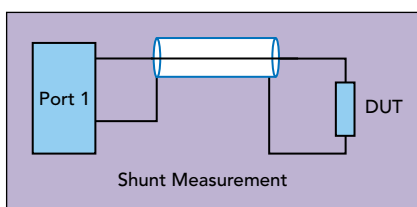
Brian Walker
Copper Mountain Technologies

A vector network analyzer (VNA) is an essential measurement tool for RF design and is often used to characterize the performance properties of filters, amplifiers, antennas, and the like. It might be surprising to learn that this versatile tool may also be used to measure and optimize the power supply systems which drive digital, analog, or RF circuits.

Possible power supply measurements include output impedance, output stability, power supply rejection ratio (PSRR), and reverse isolation. Each of these measurements are important to verify and optimize a design for best stability and noise performance. The ideal output impedance of a power supply such as a switching regulator or a low drop out (LDO) regulator is “flat” from very low frequencies to the highest frequency which is present in the circuit.

For digital circuits, this highest frequency is approximately 0.35 divided by the typical rise-time of the digital signals. Significant peaks or valleys in the output impedance are opportunities for noise development, and large peaks may indicate latent instability.

PSRR may be evaluated by injecting a signal from port 1 of a VNA into the regulator and observing the frequency response on the output as measured by port 2. Isolation, of course, is just that same measurement



▲ Fig. 1

in reverse. Both of these parameters are important. Load transients will cause voltage glitches on the output of a regulator which will make their way

through the reverse isolation and appear on the source voltage. If other regulators share this source, then those glitches will proceed through the PSRR of each of them. Clearly, it's important to understand these relationships to achieve a low noise design. Unfortunately, the power supply design is often the last consideration in a new design but being able to make fast and informative measurements to optimize the design may often avert disaster.

MEASURING LOW IMPEDANCES

A VNA measures reflection coefficients. A measurement of the reflection back to port 1 from the incident signal produced by it is called a one-port measurement and the S-Parameter is called S11. The S11 reflection coefficient is a complex number having magnitude and phase and is a function of the complex impedance, Z, being measured:

$$S_{11} = \frac{Z+Z_0}{Z-Z_0} \quad (1)$$

Where Z0 is the reference impedance of the system, typically 50 ohms.

Z may be derived from the above formula:

$$Z = \frac{Z_0(1+S_{11})}{1-S_{11}} \quad (2)$$

Schematically the measurement looks like **Figure 1**. A one-port measurement of a shunt impedance DUT using a VNA is reasonably accurate between about 20 ohms and 200 ohms. The reason for this is covered in reference 1.

A different method is required to measure the low impedances of a power supply system. A two-port

measurement is made with the unknown impedance in shunt, a “shunt-thru” measurement as shown in **Figure 2**.

The complex reflection coefficient, S21, measured in this two-port configuration is related to the complex impedance, Z of the DUT according to equation 3:

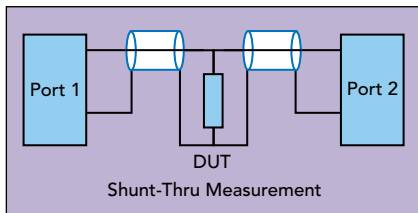
$$S_{21} = \frac{2Z}{Z_0 + 2Z} \quad (3)$$

And of course, Z can be found from the measured reflection coefficient:

$$Z = \frac{Z_0 * S_{21}}{2(1 - S_{21})} \quad (4)$$

This measurement configuration is suitable for impedance measurements from 0.001 ohms to 20 ohms. Conveniently, a two-port vector network analyzer (like the one in **Figure 3**) can make this measurement and do the impedance conversion of equation 4 in order to directly display impedance..

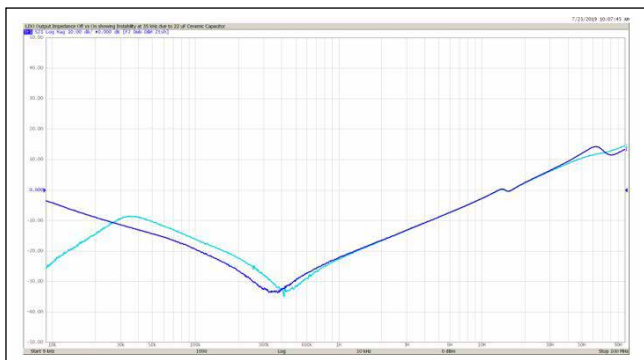
It should be noted that because the impedances measured are in shunt and low in value, the shield of the measurement cable can be a source of error. To mitigate this, a common mode choke should be attached between the DUT and port 2. For example, a model J2102B from Picotest is intended for this purpose and operates well from 1 Hz to 6 GHz



▲ Fig. 2



▲ Fig. 3 Copper Mountain Technologies S5065, 9 kHz to 6.5 GHz VNA.



▲ Fig. 4 LDO output impedance, powered and unpowered with 22 uF ceramic output capacitor.

MEASUREMENTS

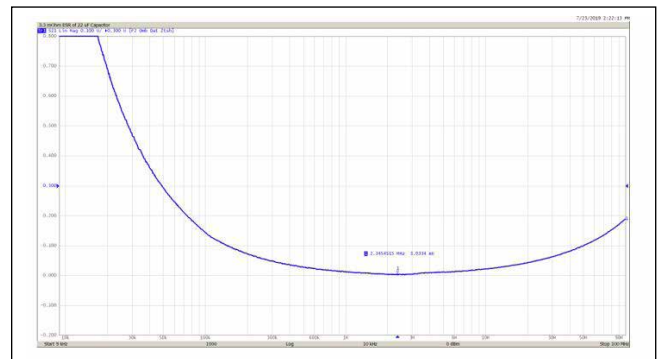
The output impedance of a low drop out (LDO) regulator will be measured with a low equivalent series resistance (ESR) 22 uF ceramic capacitor on its output with and without power applied.

The blue trace of **Figure 4** is unpowered and shows the 6 dB/octave downward slope of the 22 uF capacitor which continues until resonance at 350 kHz where the equivalent series inductance (ESL) takes over and the curve turns upward. The cyan trace depicts the output impedance with power applied. A “good” response would be flat from the lowest frequency up until resonance where the curve should then climb. Note that this chart shows ohms in dB-ohms or 20*Log(Z). The starting point of the cyan trace is -25 dB-Ohms or 0.056 Ohms. The log scale is convenient for clearly seeing the 6dB/Octave rising and falling slopes.

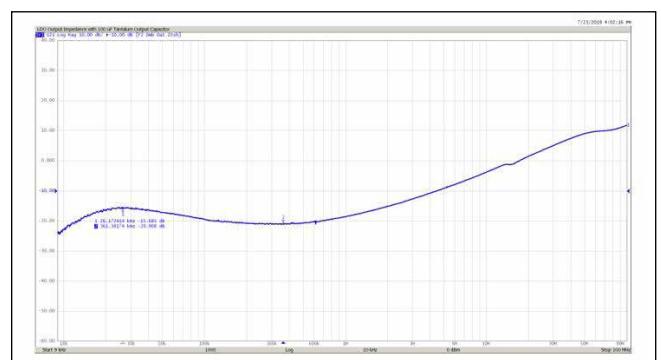
With the power on, the peaking at 35 kHz indicates instability and would result in increased system noise at this frequency throughout the circuit. It is caused by the poor choice of the low ESR ceramic output capacitor. The data sheet for the LDO specifically states that the ESR of this capacitor must be greater than 0.5 ohms. Here is a measurement of the 22 uF capacitor alone using a shunt-thru measurement.

This chart, now in linear scaling, shows the bottoming out of the 22 uF capacitor impedance as the ESR of 0.003 ohms is reached (see **Figure 5**). Clearly, we violated the design rules for this LDO circuit.

Replacing the 22 uF ceramic output capacitor with a 100 uF tantalum capacitor gives much better and flatter results as shown in **Figure 6**. This would have superior noise performance compared to the circuit with 22 uF.



▲ Fig. 5 22 uF capacitor ESR.



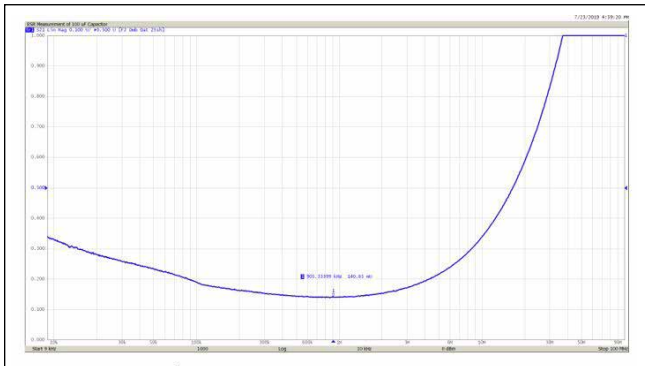
▲ Fig. 6 LDO output impedance with 100 uF Tantalum output capacitor.

Figure 7 shows the impedance of the 100 uF capacitor with linear vertical scale. The 0.140 ohm ESR is the minimum point on the curve. It isn't quite 0.5 ohms but is still an improvement. Clearly some care must be taken in the choice of regulator output filtering.

An ideal power supply system design would employ a number of capacitors with successively lower values of capacitance and ESL to bring the impedance curve back down as it begins to rise on the ESL of the next largest capacitor. It is important to manage this impedance. Trouncing it with an unplanned, over-abundance of capacity will result in "valleys" which will also result in greater system noise.

MAKING THE MEASUREMENTS

Measurement probes are useful tools for making these impedance measurements



▲ Fig. 7 ESR of 100 uF output capacitor.



▲ Fig. 8 1 port probe tip, Picotest.com.



▲ Fig. 9 Homemade probe.

| Standard | Label | Frequency | Offset | Termination |
|----------|--------------|-----------|---------|-------------|
| 1 | Open | 0 Hz | 999 GHz | 0 s |
| 2 | Short | 0 Hz | 999 GHz | 0 s |
| 3 | Load | 0 Hz | 999 GHz | 0 s |
| 4 | Unknown Thru | 0 Hz | 999 GHz | AUTO |

▲ Fig. 10 Cal kit with zeros.

Figure 8 shows the tip of a one-port measurement probe. There are also two-port probes with a single tip for making shunt-thru measurements. A homemade probe may also be constructed from simple materials. The one shown in **Figure 9** is comprised of 0.141" semi-rigid coax, a female SMA connector, and a spring pin (pogo pin). The spring pin was affixed to the coax with copper tape and then soldered. A probe such as this might be useful up to about 1 GHz. Commercially made probes like the one above will have much higher bandwidth.

For accurate impedance measurement, it is important to move the reference plane to the end of the probe. This can be done by first performing a full calibration at the cable ends and then using port extension to move the reference plane.

HOW TO DE-EMBED WITH THE S5065 VNA

The automatic port extension feature of the S5065 VNA removes the added loss of the probe. An even better calibration can be obtained by calibrating to the cable end and then de-embedding the probe. The de-embedding feature comes standard with the Copper Mountain Technologies S2VNA software).

De-embedding requires the full two-port S-Parameters of each probe. These can be obtained using the Vector Mixer Calibration feature of the VNA. First calibrate to the ends of the cables using a good mechanical calibration kit. Then create a new calibration kit entry with zeros entered for the open capacitance and short inductance and delays set to zero and select it. I named this kit "Fake". The kit entries are shown below in **Figure 10**.

This kit assumes that the short and open will be applied directly to the tip of the probe with no delay and no fringing capacitance or inductance in the short. This isn't strictly true but won't greatly affect the accuracy in these measurements.

Navigate to the Vector Mixer Calibration screen and apply an open, short, and load to the tip of the probe and click the appropriate buttons. The open can be done with the probe held aloft. A short can be done by touching center and ground to a metal surface. The load can be the measurement of a 50-ohm resistor. Click the last button to save the Touchstone file which will be used for de-embedding. The VNA will automatically enable de-embedding and apply the file to the selected port. Repeat this procedure for a second probe on port 2.



This procedure is normally used for de-embedding a reference mixer in Vector Mixer Calibration but it works quite well for this purpose as well. You might wonder how the two-port parameters are derived from the one-port measurements.

The input reflection coefficient looking into a 2-port network which is terminated with load Γ_L is:

$$\Gamma_{in} = S_{11} + \frac{S_{12} + S_{21} \cdot \Gamma_L}{1 + S_{22} \cdot \Gamma_L} \quad (5)$$

If you assume that reciprocity holds for the probe then $S_{12} = S_{21}$. A fair assumption, and:

$$\Gamma_{in} = S_{11} + \frac{S_{21}^2 \cdot \Gamma_L}{1 + S_{22} \cdot \Gamma_L} \quad (6)$$

Now there are three unknowns. Apply the three known Γ_L s, open, short, and load while making the three Γ_{in} measurements and one can solve for S_{11} , S_{21} and S_{22} .

After calibration and de-embedding has been done, one can make accurate measurements at the probe tips. For the shunt-thru measurements made in Figures 4-7, a pair of probes were used with both touched to the same node of the circuit. ■

CONCLUSION

Understanding how to make and interpret power supply impedance is very useful for optimized, low noise power supply design. With a simple pair of homemade probes, it's easy to make the measurements using a compact VNA. Don't guess whether your design is optimal when you can measure it directly!

References

1. Brian Walker, "Make Accurate Impedance Measurements Using a VNA", *Microwaves & RF*, July 2019, pp. 30-36
2. A.A. Savin, V.G. Guba, O.N. Bykova, "Measurement of Electronic Component Impedance Using a Vector Network Analyzer", UDC 621.317.33

1-Port Line Up to 18 GHz



CMT's patented 1-Port VNAs (cable and antenna analyzers) perform lab quality measurements connecting directly to the DUT without the need for a test cable (Patent US 9,291,657). The result is increased accuracy and quality of VNA measurements with a handheld instrument.

LEARN MORE



1.35 mm Precision Coaxial Connector Enables High Performance E-Band Cable Assemblies

Daniel Barnett
Teledyne Storm Microwave, Woodridge, Ill.

Hans-Ulrich Nickel
SPINNER GmbH, Munich, Germany

The 1.35 mm connector was created in response to the need for a robust mechanical connector for commercial opportunities up to E-Band, such as satellite and mobile communications and automotive.

Moore's Law was named after Gordon Moore, cofounder of Intel. In 1965, Moore observed that the number of transistors in a dense integrated circuit doubled about every year. By 1975, the industry unofficially dubbed this Moore's Law, and Moore modified his prediction to state the doubling would occur every two years.

A similar, less formalized axiom in the world of connectors is a relationship to frequency. In the early 1960s, the 14 mm precision connector was developed to operate to 8.5 GHz, followed by a succession of connector designs to reach higher frequencies: 7 mm, precision Type N, 3.50 mm, 2.92 mm, 2.40 mm, 1.85 mm and 1.00 mm. A loose corollary to Moore's Law was a 20 to 30 percent increase in frequency with each new connector design. The final leap between the 1.85 mm connector, with a maximum frequency of 65 GHz, to the 1.00 mm connector, with a maximum frequency of 110 GHz and encompassing both E- and W-Bands, is a 70 percent increase in frequency. This double band jump left an opening for a connector for E-Band. Twenty years later when the 1.00 mm connector was commercialized and some deficiencies were realized, the characteristics and design of the 1.35 mm connector was conceived.

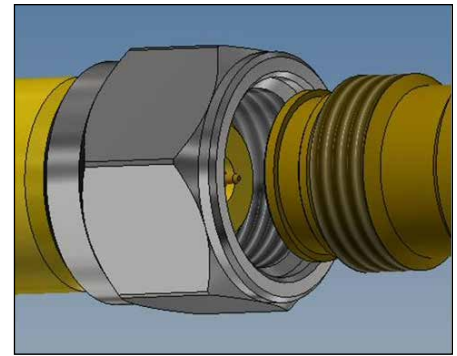
Technological innovations are typically driven by research or a commercial application and a corresponding

industry supplier. For 1.00 mm connectors, the supplier was Hewlett-Packard, and the connector was formally proposed as a standard (IEEE Std 287-2007) in 1989. However, the first commercial quantities of 1.00 mm connectors were not available until 2010. At higher frequencies, physics constrains the implementation of features such as captivation and connector thread pitch, and the size associated with these higher frequencies results in the 1.00 mm connector being less rugged. Initially, this was not a problem, since the users comprised mostly research facilities that understood how to handle sensitive connectors and cable assemblies.

With deregulation of these frequency bands and applications becoming more cost effective, the commercial world has begun to realize the potential. A group of commercial applications, namely automotive and satellite/mobile communications, reside below 90 GHz in E-Band, and they require large numbers of assemblies that must also be rugged and cost effective. In 2014, SPINNER GmbH decided these applications would benefit from a rugged connector with some but not all of the W-Band connector attributes. Leveraging V- and W-Band connector design features, SPINNER began developing a 1.35 mm E-Band connector with the more rugged construction of the V connector and broadband performance to at least 90 GHz. SPINNER teamed with Physikalisch-

| TABLE 1 | | | |
|---|----------------------------------|----------------------------------|----------------------------------|
| CONNECTOR REQUIREMENT AND CONFORMITY | | | |
| Requirement | 1.85 mm (V Connector) | 1.35 mm (E Connector) | 1.00 mm (W Connector) |
| Pin and Socket Design with Air Dielectric Interface | | | |
| Two Different Connector Quality Levels (Like the IEEE "Metrology Grade" and "Instrument Grade") | | | |
| Upper Operating Frequency of ≥ 90 GHz | 65 (70) GHz | 90 (92) GHz | 110 (120) GHz |
| Robust Design: Not Over-Miniaturized, Big Centering Cylinder & Large Contact Surface | | | |
| Fine Threaded Coupling Nut Prevents Loosening | M7 x 0.75 | M5.5 x 0.5 | M4 x 0.7 |
| Socket Connector Equipped with Locking Groove to Allow for Push-On Pin Connector | | | |
| "Thru Male" Capability with a Standard Semi-Rigid Cable | 0.086 in. | 0.047 in. | |
| Applicable Locking Torque of 1.6 Nm without Plastic Deformation of Outer Conductor | | | |
| Coupling Nut with Flat Size of 8 mm | | 7 or 6.35 mm Option | 6 mm |
| Accepts Same Wrench as the 3.50, 2.92 and 2.40 mm Connectors (Equal Size and Torque) | | | |

(GREEN = CONFORM, RED = NOT CONFORM)



▲ Fig. 1 1.35 mm connector pin and socket.

Technische Bundesanstalt, the national metrological institute of Germany; Rosenberger; and Rohde & Schwarz to define and develop the 1.35 mm interface. The resulting design was proposed to the IEEE P287 committee, a group revising the IEEE Std 287-2007 for precision coaxial connectors, which decided to include the 1.35 mm connector in the next edition of the standard. In parallel, the interface design was also submitted to IEC, which will publish it as IEC 61169-65.

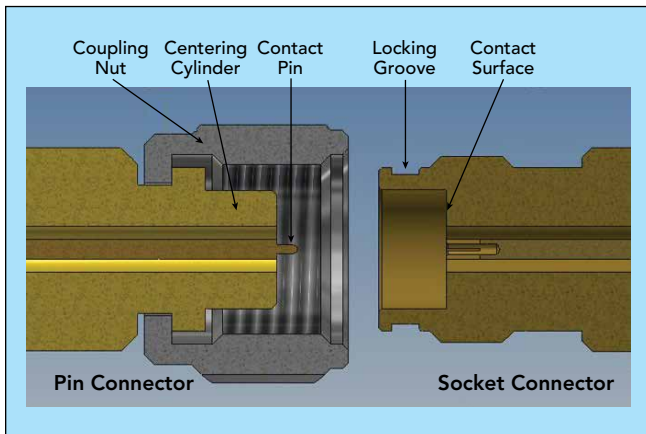
1.35 MM CONNECTOR DESIGN

For the 1.35 mm connector interface, several development requirements were defined and realized (see **Table 1**). The table shows the requirements, comparing them with the other two existing connectors (1.85 mm and 1.00 mm) covering the adjacent frequency bands. **Tables 2** and **3** are extracts from the 1.35 mm connector's electrical and mechanical interface specifications, respectively. The complete specifications and all drawings will be published in the next edition of the IEEE Standard.

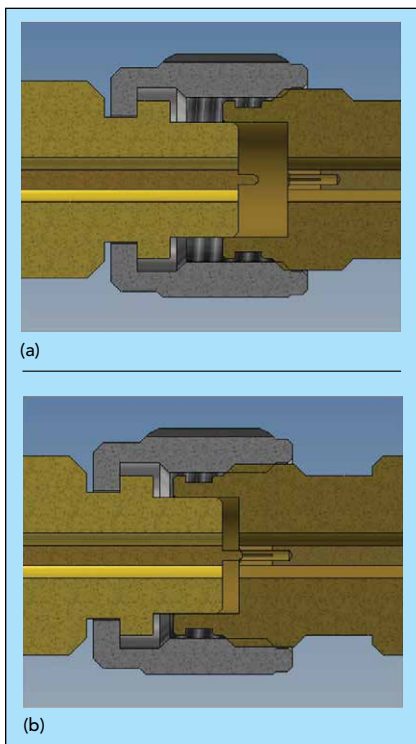
A 3D view of the 1.35 mm interface is shown in **Figures 1** and **2**. The overall design avoids any unnecessary over-miniaturization, making it strong and robust, even for a frequently used front panel connector on a test instrument. The pin connector features a relatively large centering sleeve (3.5 mm \times 2.6 mm). When the pin and socket connectors are mated, the outer conductor is guided precisely before the center conductors make contact (see **Figure 3**). The large size of the centering sleeve together with the fine thread (M5.5 \times 0.5) of the coupling nut ensures the robustness of the interface. The interface has a large contact surface to avoid plastic deformation of the contact area, even when operated

| TABLE 2 | | |
|--|-------------------------|------------------------|
| 1.35 MM CONNECTOR ELECTRICAL SPECIFICATIONS | | |
| Description | Instrument Grade | Metrology Grade |
| Characteristic Impedance | $50 \pm 0.25 \Omega$ | $50 \pm 0.15 \Omega$ |
| Guaranteed Upper Operating Frequency | 90 GHz | |
| Unsupported Air Line H_{11} Cutoff Frequency | 98.5 GHz | |
| $ S_{11} $ | -20 dB | -24 dB |
| $ S_{11} $ Repeatability | -43 dB | -48 dB |
| Insertion Loss | 0.05 dB | |
| Insertion Loss Repeatability | 0.03 dB at 90 GHz | |
| Transmission Phase Repeatability | 1° at 90 GHz | |
| Electrical Length Tolerance | $\pm 75 \mu\text{m}$ | |
| Shielding Effectiveness | -90 dB | |

| TABLE 3 | |
|--|--|
| 1.35 MM CONNECTOR MECHANICAL SPECIFICATIONS | |
| Description | Specification |
| Outer Conductor Inside Diameter | 1.35 mm (0.053 in) |
| Inner Conductor Outside Diameter | 0.586 mm (0.023 in) |
| Connect/Disconnect Life | 3000 cycles |
| Coupling Torque | 0.9 Nm (8.0 in-lb) |
| Maximum Safety Torque | 1.65 Nm (14.6 in-lb) |
| Coupling Thread | M5.5 \times 0.5 |
| Coupling Nut Wrench Size | 8 mm (7 or 6.35 mm for Special Applications) |



▲ Fig. 2 Longitudinal cross-section of the 1.35 mm pin and socket.



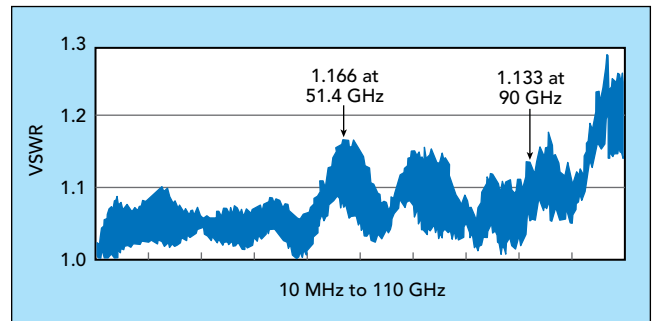
▲ Fig. 3 1.35 mm connector mating, showing engagement of the outer conductor centering cylinder (a) and engagement of the inner conductor pin (b).

a standard locking groove, which allows mating with an optional push-on type pin connector.

CABLE ASSEMBLY CHALLENGES AND CHOICES

In the world of mmWave connectors, the three cornerstones of design are tolerances, tolerances and tolerances. From the previous connector design discussion, dimensional integrity was enforced with various design choices, such as a centering sleeve on the pin side and a locking groove on the socket side. The connector is created from several machined parts whose dimensional integrity is limited by the sophistication and precision of the machining process. For a cable assembly there are additional factors, including cable construction, cable preparation (i.e., stripping

with a maximum locking torque of 1.6 Nm (14.6 in-lb). This is the precondition for the operational coupling torque of 0.9 Nm (8.0 in-lb), which is the same as for the lower frequency 3.50, 2.92, 2.40 and 1.85 mm connectors. The diameter of the contact pin is equal to the nominal center conductor diameter of a standard 0.047 in. semirigid cable (MIL-DTL-17/151). This feature enables the design of high quality, low budget “thru male” pin connectors. The 1.35 mm socket connector is equipped with



▲ Fig. 4 1.35 mm cable assembly VSWR measured with 1.35 to 1.00 mm adapters gated out of the measurement.

three layers: the inner conductor, outer conductor and outer braid) and soldering the layers. The machined connector parts are metal (e.g., stainless steel and beryllium copper) and harder plastics (e.g., Ultem) that are manufactured to defined tolerances.

Applying tolerances to a cable that consists of multiple layers and materials that move in relation to one another, as well as applying heat to a solder joint, requires art as well as science. There are multiple, established cable designs; for this application, the combination of an extruded PTFE core for strength and robustness, a helical wrap outer conductor for superior electrical performance and stability and an outer braid for strength were chosen. Initial testing revealed electrical performance instabilities at E-Band that were not apparent at V-Band and below. Adding a layer between the outer conductor and the outer braid reinforced the rotational integrity of the helical wrap, providing extra dimensional support and eliminating the instabilities.

The solution to this problem underscores the known difficulty of the preparation and termination of a cable with a tape layer to the cable entry portion of the connector. This involves consideration of the tolerances for each of the strip lengths of the individual cable layers, i.e., the inner conductor, outer conductor and outer braid. In addition, each individual layer consists of a different base material, which necessitates a tailored stripping approach. While the intellectual understanding of soldering a two-stage ferrule is well understood, at mmWave wavelengths an iterative termination process was required—each time improving, learning and discovering. While the science of thoroughly documenting each step is important, equally important is the art of the skilled, experienced and intuitive technician.

The confluence of art and science is even more crucial in the soldering process. There is no concept of a precise application of heat in a non-automated soldering process, which is how the 1.35 mm cable assemblies are manufactured. Also, there are many dissimilar materials in the cable construction (e.g., PTFE, steel and copper) with individual coefficients of thermal expansion and minutely non-symmetrical construction (e.g., a helical wrap that creates an internal spiral to mimic a smooth cylinder). L- through Q-Band cable constructions are more forgiving to the application of heat and the imprecision of the mechanical connections. Starting with V-Band and quite dramatically at E- and W-Band, small mechanical variations translate to electrical performance degradation.

There are effectively a series of micro-environments in the cable to connector interface, starting with the soldering of the outer braid portion of the ferrule, proceeding to the outer conductor portion of the ferrule and transitioning to the rear portion of the connector. The goal is to keep each of these sections as close to $50\ \Omega$ as possible. If there must be an impedance difference in the connector, the transition should be gradual. When soldering the cable to the connector, the heat expands the PTFE dielectric. For this size cable (0.055 in. diam-

eter) a 1 mil change in the diameter of the extruded dielectric results in a change of $1\ \Omega$. In practice, analyzing and compensating each micro-environment of impedance is not possible. What is possible is honing the manufacturing process by minimizing heat and creating tooling that enables precise trimming and measurement during cable preparation. Then the manufacturing technicians use their accumulated skills and experience to manufacture the cable.

PERFORMANCE

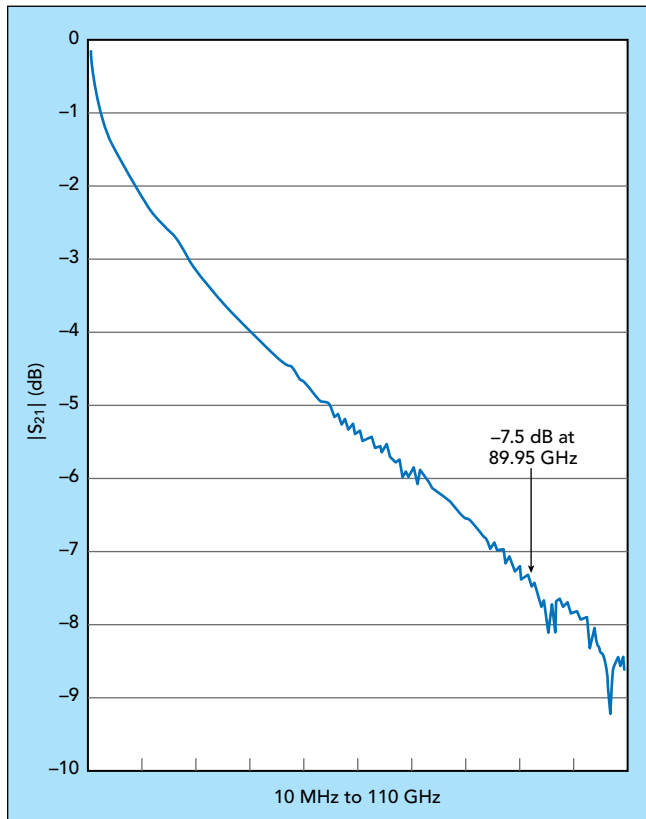
The following data represents the performance of connector in pre-production. **Figure 4** shows the broadband VSWR response; the highest VSWR is 1.16:1 at 51 GHz, dropping slightly to 1.13:1 at the upper frequency of 90 GHz. When these measurements were made, the 1.35 mm calibration kit was still being developed (it has since been finished), so the VNA was calibrated to 110 GHz using 1.35 to 1.00 mm adapters over the full bandwidth. To eliminate the contribution of the adapters, the calibration comprised 11,000 points to use the VNA's gating function. The VSWR readings are gated to the end of the pair of adapters. The insertion loss of the cable assembly is plotted in **Figure 5**. Table 2 specifies the upper frequency to be 90 GHz and the theoretical cut-off to be 98.5 GHz. From the data, the connector modes close to 98 GHz.

Figure 6 shows the time domain performance of the cable, which quantifies impedance mismatches at different sections of the assembly out to 800 ps, which includes the end of the VNA test port, the adapters, the connector and a portion of the cable. The Y axis shows the impedance deviation from $50\ \Omega$. The calibration point at 0 ps is at $50\ \Omega$. Between markers 1 and 2 is the 1.00 mm to 1.35 mm adapter, which is matched to the network analyzer and connector. Before marker 3, which is at the end of the ferrule section of the connector, there is a $2\ \Omega$ mismatch caused by dielectric expansion, which occurred when the ferrule was heated for soldering. Fine tuning this pre-production connector design included changing the inner diameter of the ferrule, with a 1 mil change lowering the inductive reflection and improving the VSWR.

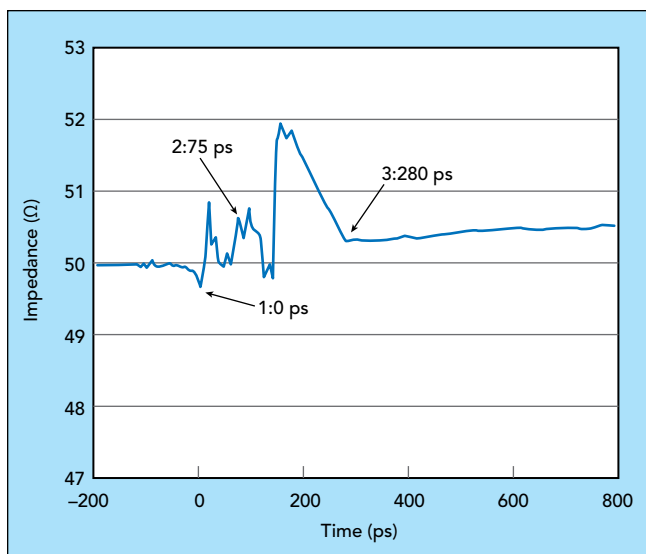
LAUNCHING THE 1.35 MM FAMILY

With the connector and cable development complete, the cable assembly and manufacturing processes are being fine-tuned to support an early October product launch. The 1.35 mm connector system—comprising the calibration kit, rotary joint, inter-series adapter, printed circuit board connectors and cable assemblies—are available. Near-term development plans include a waveguide to 1.35 mm adapter for hybrid applications.

The 1.35 mm connector was created to fill the need for a robust mechanical connector “up to E-Band,” to support the satellite and mobile communications and automotive sectors. The commercial release follows a five-year gestation from the definition of standards to the availability of products. The evolution of connector technology will continue, with 5G and future generations anticipating systems operating to 140 GHz—driving the exploration of a commercial 0.8 mm connector.■



▲ Fig. 5 Measured $|S_{21}|$ including the 1.35 to 1.00 mm adapters.



▲ Fig. 6 Time domain measurement of the connector showing a $2\ \Omega$ mismatch, caused by dielectric expansion when the ferrule was heated for soldering.



Original Metrology-Grade USB VNAs EXTEND YOUR REACH[®] since 2011

2011 ● First Metrology-Grade USB VNA



2012 ● Handheld USB VNA that Requires No Measurement Cable (US Patent 9,291,657)

2013 ● Direct Receiver Access USB VNAs



2014 ● Compact USB VNAs

2015 ● 20 GHz USB VNAs with 135 dB Dynamic Range and 10 μs Measurement Speed



2016 ● 50-110 GHz Frequency Extension System Anchored by 9 GHz USB VNA



2017 ● 18 GHz 1-Port USB VNA



18-54 GHz Frequency Extender for 5G Applications

2018 ● Portable Materials Measurements Solution up to 6 GHz
VNA Software for Linux[®] Operating System



Affordable M Series VNAs to 18 GHz

2019 ● 2-port 9 GHz VNA for National Instruments' PXI System
Advanced Performance Compact VNA - SC Series



LEARN MORE cpmt.link/37g3qqi

Linux[®] is the registered trademark of Linus Torvalds in the U.S. and other countries.